



# DeLiAn – a growing collection of depolarization ratio, lidar ratio and Ångström exponent for different aerosol types and mixtures from ground-based lidar observations

Athena Augusta Floutsi<sup>1</sup>, Holger Baars<sup>1</sup>, Ronny Engelmann<sup>1</sup>, Dietrich Althausen<sup>1</sup>, Albert Ansmann<sup>1</sup>, Stephanie Bohlmann<sup>1,a</sup>, Birgit Heese<sup>1</sup>, Julian Hofer<sup>1</sup>, Thomas Kanitz<sup>1,b</sup>, Moritz Haarig<sup>1</sup>, Kevin Ohneiser<sup>1</sup>, Martin Radenz<sup>1</sup>, Patric Seifert<sup>1</sup>, Annett Skupin<sup>1</sup>, Zhenping Yin<sup>1,2</sup>, Sabur F. Abdullaev<sup>3</sup>, Mika Komppula<sup>4</sup>, Maria Filioglou<sup>4</sup>, Elina Giannakaki<sup>4,5</sup>, Iwona S. Stachlewska<sup>6</sup>, Lucja Janicka<sup>6</sup>, Daniele Bortoli<sup>7</sup>, Eleni Marinou<sup>8</sup>, Vassilis Amiridis<sup>8</sup>, Anna Gialitaki<sup>8,9,c</sup>, Rodanthi-Elisavet Mamouri<sup>10,11</sup>, Boris Barja<sup>12</sup>, and Ulla Wandinger<sup>1</sup>

<sup>1</sup>Leibniz Institute for Tropospheric Research (TROPOS), Leipzig, Germany

<sup>2</sup>School of Remote Sensing and Information Engineering, Wuhan University, Wuhan, China

<sup>3</sup>Physical Technical Institute of the National Academy of Sciences of Tajikistan, Dushanbe, Tajikistan

<sup>4</sup>Finnish Meteorological Institute, Kuopio, Finland

<sup>5</sup>Department of Environmental Physics and Meteorology, University of Athens, Athens, Greece

<sup>6</sup>Faculty of Physics, University of Warsaw, Warsaw, Poland

<sup>7</sup>Évora University, Institute for Earth Sciences, Évora, Portugal

<sup>8</sup>IAASARS, National Observatory of Athens, Athens, Greece

<sup>9</sup>Laboratory of Atmospheric Physics, Physics Department, Aristotle University of Thessaloniki, Thessaloniki, Greece

<sup>10</sup>ERATOSTHENES Centre of Excellence, Limassol, Cyprus

<sup>11</sup>Cyprus University of Technology, Department of Civil Engineering and Geomatics, Cyprus

<sup>12</sup>Atmospheric Research Laboratory, University of Magallanes, Punta Arenas, Chile

<sup>a</sup>now at: Finnish Meteorological Institute, Helsinki, Finland

<sup>b</sup>now at: European Space Agency, ESTEC, Noordwijk, the Netherlands

<sup>c</sup>now at: School of Physics and Astronomy, Earth Observation Science Group, University of Leicester, Leicester, UK

**Correspondence:** Athena Augusta Floutsi (floutsi@tropos.de)

**Abstract.** This paper presents a collection of lidar-derived aerosol intensive optical properties for several aerosol types, namely the particle linear depolarization ratio, the extinction-to-backscatter ratio (lidar ratio) and the Ångström exponent. The data collection, named DeLiAn, is based on globally distributed, long-term, ground-based, multiwavelength, Raman and polarisation lidar measurements, conducted mainly with lidars that have been developed at the Leibniz Institute for Tropospheric Research.

- 5 The intensive optical properties are presented at two wavelengths, 355 and 532 nm, for 13 aerosol categories. The categories cover the basic aerosol types (i.e., marine, pollution, continental European background, volcanic ash, smoke, mineral dust) as well as the most frequently observed mixtures they form. This extensive collection also incorporates more peculiar aerosol categories, including dried marine aerosol that, compared to marine aerosol, exhibits a significantly enhanced depolarization ratio (up to 15%). Besides Saharan dust, additional mineral dust types related to their source region were identified due to their
- 10 lower lidar ratios (Central Asian and Middle Eastern dust). In addition, extreme wildfire events (such as in north America and Australia) emitted smoke into the stratosphere showing significant different optical properties, i.e., high depolarization values



(up to 25%), compared to tropospheric smoke. The data collection reflects and underlines the variety of aerosol mixtures in the atmosphere and can be used for the development of aerosol typing schemes. The paper contains the currently most comprehensive overview of optical properties from aerosol lidar measurements and, therefore, provides a solid basis for future aerosol retrievals in the frame of both spaceborne and ground-based lidars. Furthermore, DeLiAn can assist the efforts for harmonization of satellite records of aerosol properties performed at different wavelengths.

## 1 Introduction

Aerosol typing is intertwined with the scientific efforts for the quantification of the direct and indirect aerosol radiative effects, the identification of the main aerosol sources and the improvement of the aerosol measurements, retrievals and models. All these efforts have a common baseline: the reduction of the aerosol-induced uncertainties in the Earth's radiative budget (Boucher et al., 2013). The uncertainties are directly linked to the physico-chemical properties and the spatiotemporal variability of the aerosol particles.

The climate response to aerosols is not only type- but also altitude-dependent and, therefore, the vertical aerosol distribution is a key factor for the evaluation of the direct aerosol radiative effect (Hansen et al., 1997). Lidars are the only instruments that can accurately characterize complex aerosol mixtures as they provide information on the optical and microphysical properties of different aerosol types along with their vertical distribution (Ansmann and Müller, 2005). Lidar-derived intensive optical parameters can be used effectively for aerosol-typing purposes because, in contrast to extensive properties, they are concentration-independent. The extinction-to-backscatter ratio (lidar ratio), the particle linear depolarization ratio and the Ångström exponent (backscatter- and extinction-related) reveal information about the size, shape and absorption efficiency of the aerosol particles. The combination of different lidar-derived intensive optical properties is proven to be a sophisticated way for the classification of the different aerosol types and their mixtures (e.g., Sasano and Browell, 1989; Sugimoto et al., 2002; Ansmann et al., 2002; Müller et al., 2002, 2003, 2005; Mattis et al., 2002b, 2004; Tesche et al., 2009b, 2011a; Groß et al., 2011, 2013; Weinzierl et al., 2011; Burton et al., 2012; Papagiannopoulos et al., 2018; Nicolae et al., 2018). Especially the combination of the particle linear depolarization ratio and the lidar ratio is highly effective for classification purposes, since those parameters exhibit the highest discrimination power among the lidar-derived intensive optical parameters (Burton et al., 2012).

Due to the high capabilities of the lidar instruments with respect to aerosol monitoring and characterization, several lidar networks have emerged around the globe in the last decades. The Micro-Pulse Lidar Network (MPLNET) of the National Aeronautics and Space Administration (NASA) has sites mainly across North America (Welton et al., 2002), the Asian Dust and Aerosol Lidar Observation Network (AD-Net) is expanding in East Asia (Sugimoto et al., 2014), the Latin-American Lidar Network (LALINET) over Latin America (Antuña-Marrero et al., 2017) and most parts of Europe are covered by the European Aerosol Research Lidar Network (EARLINET; Pappalardo et al., 2014). These networks operate different lidar systems and therefore have different capabilities. For instance, MPLNET is equipped with an elastic-backscatter lidar that operates at 532 nm. AD-Net is mostly equipped with Raman lidars operational mainly at 532 and 1064 nm. Similarly, EARLINET stations



45 are mostly equipped with multiwavelength (355, 532 and 1064 nm) Raman lidars. Elastic lidar systems have limited capabilities  
(e.g., with respect to aerosol typing) compared to Raman lidar systems, since two physical quantities, the particle backscatter  
and extinction coefficients, need to be determined by one measured quantity, i.e., the elastic lidar return (Ansmann and Müller,  
2005). On the other hand, with the Raman lidar method (Ansmann et al., 1992) the backscatter and extinction coefficients can  
be determined independently. In addition, spectral information provided by multiwavelength lidars advance aerosol typing and  
50 can be used to derive microphysical particle properties (via inverse modelling).

Since the 90s, the Leibniz Institute for Tropospheric Research (TROPOS) has conducted extensive research on the topic of  
lidar and aerosols. Two complex lidar systems named MARTHA and BERTHA have been developed using several different  
lidar-specific techniques (Raman, polarization, multi-wavelength, high-spectral-resolution, etc.) throughout the years. The mo-  
bile container-based BERTHA (Althausen et al., 2000) was deployed at several field campaigns since the end of the 1990's  
55 (e.g., LACE98 (Wendisch et al., 2002), ACE-2 (Ansmann et al., 2002), INDOEX (Ansmann et al., 2000), COPS (Herold et al.,  
2011), SAMUM 1&2 (Ansmann et al., 2011), SALTRACE (Haarig et al., 2017a)), while the lab-based MARTHA (Mattis et al.,  
2002a) was used for EARLINET observations (Mattis et al., 2004, 2008) and testing of new methodologies (e.g., Mattis et al.,  
2002a; Schmidt et al., 2013; Jimenez et al., 2020a). In parallel, novel data retrieval techniques have been developed and steadily  
improved, which are meanwhile state-of-the-art for active aerosol profiling (Ansmann and Müller, 2005), e.g., inversion tech-  
60 niques (Müller et al., 1998), separation of aerosol components with polarization (POLIPHON, Mamouri and Ansmann, 2016),  
automatic and unsupervised data retrievals (e.g., Baars et al., 2008, 2016; D'Amico et al., 2015; Baars and Yin, 2020; Yin  
and Baars, 2021). The intensive work on the inversion technique methodology (e.g., Müller et al., 1999a, b, 2000, 2011) led  
finally to the conclusion that 3+2 lidars (backscatter coefficient at three wavelengths, extinction coefficient at two wavelengths)  
are needed as ideal setup for remote sensing of aerosol microphysical properties – a conclusion which is meanwhile also ap-  
65 plied in EARLINET and ACTRIS (Aerosol, Clouds and Trace Gases Research Infrastructure). The introduction and intense  
use of the polarization technique led to the possibilities to separate dust and non-dust components (Teschke et al., 2011a), fine  
and coarse mode of dust (Mamouri and Ansmann, 2014) and even to the retrieval of CCN (Cloud Condensation Nuclei) and  
INP (Ice Nucleating Particles) properties (Mamouri and Ansmann, 2015, 2016) – important parameters to investigate aerosol-  
cloud-interactions. Also these techniques are meanwhile widely standardized applied in ACTRIS and beyond. Based on the  
70 experience and expertise gathered in the 90s and with the upcoming need for automatized observations, in 2002, the first portable,  
remotely controlled, multiwavelength Raman polarization lidar system (Polly) was developed at TROPOS (Althausen et al.,  
2009; Engelmann et al., 2016). Since then, more than a dozen lidars of Polly/Polly<sup>XT</sup> type (more details in Sect. 2.1; Engel-  
mann et al., 2016) have been constructed and are operating within the framework of a voluntary, scientific network called  
PollyNET (Baars et al., 2016). The mobility of Polly<sup>XT</sup> systems as well as their automated and continuous 24/7 observational  
75 capabilities make them ideal for deployment in remote places during measurement campaigns (e.g., the Amazon (Baars et al.,  
2012), China (Hänel et al., 2012; Heese et al., 2016), South Africa (Giannakaki et al., 2016), India (Komppula et al., 2012),  
and more recently in Cyprus (Ansmann et al., 2019), the Arctic (Engelmann et al., 2021) and Punta Arenas, Chile (Radenz  
et al., 2021a)) and on research vessels, such as Sonne, Meteor (Rittmeister et al., 2017) and Polarstern (Kanitz et al., 2013a;  
Bohlmann et al., 2018).



80 Lidars have also been successfully deployed in space, aiming to contribute to the scientific efforts for atmospheric measure-  
ments on a global scale. For a remarkable duration of 16 years, CALIOP (Cloud-Aerosol Lidar with Orthogonal Polarization)  
on board NASA's CALIPSO (Cloud-Aerosol Lidar and Infrared Pathfinder Satellite Observations) has measured vertical pro-  
files of attenuated backscatter at visible and near-infrared wavelengths, along with depolarization in the visible channel (Winker  
et al., 2009). However, as an elastic-backscatter lidar, CALIOP is not able to perform direct extinction measurements. To enable  
85 the retrieval of the backscatter and extinction coefficients from the attenuated backscatter signals, the lidar ratio needs to be  
assumed. Since the lidar ratio depends on the aerosol types present in the atmosphere, an aerosol typing scheme was developed  
for CALIPSO (Omar et al., 2005, 2009; Kim et al., 2018).

In 2018, the European Space Agency (ESA) launched the wind lidar mission Aeolus (Stoffelen et al., 2005). The satellite  
is equipped with a 355-nm high-spectral-resolution lidar (HSRL), the Atmospheric Laser Doppler Instrument (ALADIN).  
90 ALADIN is the first wind lidar in space and its HSRL capabilities provide also the first direct-measured extinction profiles  
and aerosol optical properties from space, as a spin-off product (Flament et al., 2021), as already successfully demonstrated in  
Baars et al. (2021). This is a great step towards the harmonization of multiple satellite instruments, especially with view on the  
upcoming Cloud, Aerosol and Radiation Explorer (EarthCARE) joint mission of ESA and the Japanese Aerospace Exploration  
Agency (JAXA), scheduled for launch in 2023.

95 EarthCARE's payload consists of four instruments: an ATmospheric LIDar (ATLID), a Cloud Profiling Radar (CPR), a  
Multi-Spectral Imager (MSI) and a Broad-Band Radiometer (BBR) (Illingworth et al., 2015). ATLID is a 355-nm HSRL that  
will provide direct cloud and aerosol profile measurements of backscatter and extinction coefficients. Furthermore, ATLID is  
able to measure the depolarization ratio of the atmospheric particles – an ideal parameter for aerosol typing – as well as ice  
particle characteristics (Illingworth et al., 2015; do Carmo et al., 2021). The primary goal of EarthCARE is radiative closure,  
100 which is aimed to be achieved in a synergistic approach from the two active and two passive instruments. One key element for  
this goal is a proper aerosol typing scheme, to calculate the aerosol's radiative properties. For this purpose, the Hybrid End-To-  
End Aerosol Classification (HETEAC) model has been developed (Wandinger et al. 2016a, Wandinger et al. in preparation). As  
the name indicates, the HETEAC model delivers the required theoretical description of aerosol microphysics that is consistent  
with experimentally derived optical properties (hybrid approach) to close the loop from observations and aerosol microphysics  
105 to radiative properties (end-to-end approach).

It is evident that global, vertically resolved observations from ground-based and spaceborne lidars need to be harmonized  
(i.e., spectral harmonization). The harmonization of, e.g., lidar-derived intensive optical properties would improve the consis-  
tency of the lidar data obtained by different lidar systems, and would allow for comprehensive studies on the statistical relations  
between those properties. Harmonized datasets of intensive optical parameters would not only lead to the creation of robust  
110 aerosol typing algorithms, but would also improve already existing ones.

Given the need for development and improvement of aerosol typing schemes, such as HETEAC, and data harmonization  
among lidar networks (i.e., MPLNET, AD-Net, LALINET, EARLINET, PollyNET) and satellites (e.g., CALIPSO, Earth-  
CARE), in this paper, we present an experimental data collection of aerosol-type-dependent optical properties. The optical  
properties are the particle linear depolarization ratio, the lidar ratio and the Ångström exponent and, hence, the data collection



115 is named DeLiAn. The optical properties have been obtained either by lidar systems that have been developed at TROPOS (such  
as MARTHA, BERTHA, Polly<sup>XT</sup>; more information in Sec.2) or by other accompanying lidar systems (explicitly mentioned  
in Sec.2) during different field campaigns and at different locations throughout many years (see Tab. 1 and Fig.1). In addition  
to the well-known aerosol types (such as marine, dust, pollution, etc.), DeLiAn features new findings and aerosol types (e.g.,  
Central Asian dust (Hofer et al., 2020), dried marine (Haarig et al., 2017b), stratospheric smoke (Haarig et al., 2018; Ohneiser  
120 et al., 2020)) that were identified during recent measurement campaigns. The aim is to provide additional knowledge on the  
intensive aerosol properties for different aerosol types and mixtures, which in turn can be used to constrain and enhance aerosol  
retrievals.

In the following section, we briefly present the lidar systems used, information about the data handling, and we provide  
an overview of the locations where the relevant lidar systems have been operated. In Section 3, the collection of the lidar-  
125 derived intensive optical parameters (DeLiAn) is presented and discussed in detail with respect to the different aerosol types  
and mixtures. The statistical analysis performed is also presented in the same section along with comparisons between the  
optical properties used for the CALIPSO aerosol typing scheme and the respective ground-based ones that were obtained from  
the present study. The conclusions and an outlook finalize the paper.

## 2 Instruments, data analysis and sources

### 130 2.1 Lidar systems

#### 2.1.1 MARTHA

The Multiwavelength Aerosol Raman Lidar for Temperature, Humidity, and Aerosol profiling is a lab-based lidar of TROPOS  
that has been used not only for acquiring cloud and aerosol measurements but also for testing new methodologies (Mattis  
et al., 2002a; Schmidt et al., 2013; Jimenez et al., 2019, 2020a). MARTHA's powerful laser together with its large prime mirror  
135 (80 cm in diameter) makes it ideal for tropospheric and stratospheric aerosol observations, and recently has been upgraded to a  
dual-receiver-field-of-view lidar (RFOV; Jimenez et al., 2020b). The operational setup has been steadily changed but covers at  
least  $3\beta + 2\alpha + \delta$  (three backscatter coefficients at 355, 532 and 1064 nm, two extinction coefficients at 355, 532 nm and one  
depolarization ratio at 532 nm). MARTHA is part of EARLINET/ACTRIS (Pappalardo et al., 2014) but not yet automatized.

#### 2.1.2 BERTHA

140 The Backscatter Extinction lidar-Ratio Temperature Humidity profiling Apparatus (BERTHA) is the oldest mobile, container-  
based multiwavelength polarization Raman lidar of TROPOS (Althausen et al., 2000). For 25 years, BERTHA has been pro-  
viding extensive and intensive aerosol optical properties and has been deployed at numerous field campaigns (most notably  
in both the SAMUM and SALTRACE field experiments, more details in Sec.2.2). Manual operation is needed for this lidar.  
A distinctive feature of this lidar system is that since 2012, it enables simultaneous measurements of the depolarization ratio  
145 at three wavelengths (355, 532 and 1064 nm). In 2015 the setup was extended by the first measurements of the extinction



coefficient at 1064 nm, leading to a  $3\beta + 3\alpha + 3\delta$  setup (three backscatter coefficients, three extinction coefficients and three depolarization ratios). The system includes a water vapor and a HSRL channel (407 and 532 nm, respectively). For a more detailed description of the latest setup of the lidar system readers may refer to Haarig et al. (2016, 2017a).

### 2.1.3 Polly<sup>XT</sup> lidar systems

150 Since the first Polly system (Althausen et al., 2009) was assembled in 2002, more than a dozen lidars of Polly/Polly<sup>XT</sup> type have been constructed at TROPOS, with continuous upgrading efforts (Engelmann et al., 2016), and deployed either permanently or temporarily at measurement campaigns and research vessels (for visualization see the online map at [polly.tropos.de](http://polly.tropos.de), last access: 18 October 2022). Some Polly<sup>XT</sup> lidars are part of EARLINET/ACTRIS (Pappalardo et al., 2014). Polly<sup>XT</sup> Raman lidars emit light at three different wavelengths, 355, 532 and 1064 nm. The lidars are nowadays equipped with a receiver that  
155 consists of twelve or more channels, which enable measurements of the elastically (355, 532, 1064 nm) and Raman-scattered light (387, 607 nm for aerosols and 407 nm for water vapour) and the depolarization state of the backscatter light (at 355 and 532 nm). The near-range telescope allows the detection of scattered light (at 355, 387, 532 and 607 nm) from an altitude of around 60–80 m above ground level (AGL). The uppermost detection height for the vertical profiles is around 20 km AGL. Data from all channels are acquired with a vertical resolution of 7.5 m and a temporal resolution of 30 s (for more details refer  
160 to Engelmann et al., 2016).

This setup allows the determination of extensive and intensive aerosol optical properties, which are important quantities for the monitoring and characterization of the aerosol. The determination of the backscatter coefficient (355, 532 and 1064 nm) and the extinction coefficient (355 and 532 nm) leads to the lidar ratio and Ångström exponent (Baars et al., 2016). Another intensive optical property, the particle linear depolarization ratio, defined as the cross-polarized-to-co-polarized backscatter  
165 ratio (orthogonal and parallel planes of polarization to the plane of linear polarization of the transmitted laser pulses, respectively), is also determined (Baars et al., 2016). Quality assurance procedures are a key aspect for lidars (e.g., Bravo-Aranda et al. 2016; Wandinger et al. 2016b; Freudenthaler 2016; Belegante et al. 2018; Freudenthaler et al. 2018) and the Polly<sup>XT</sup> lidar systems and data processing follows the EARLINET standards even when the lidars are operated at non-stationary sites (e.g., on research vessels). Near-real-time (NRT) quicklooks can be found at [polly.tropos.de](http://polly.tropos.de) (last access: 18 October 2022).

## 170 2.2 Lidar data analysis, locations and sources

The data collection presented here comprises various measurements from several locations, an overview is given in Fig. 1. We have considered data that are already published (layer- and observational-mean values) and added additionally analyzed data for specific aerosol types. The evaluation of the published lidar data has been performed by the authors of the corresponding papers. The full list of the respective references can be found in Tab. 1, while a brief description of the major field campaigns  
175 mentioned in the same table is provided below.

Table 1 provides an overview of all the aerosol types that were considered during the creation of DeLiAn. It corroborates previous findings and provides new insights regarding aerosol types based on recent measurement campaigns and studies.



**Table 1.** Overview of the lidar-derived optical properties of different aerosol types. The lidar ratio  $S$  is expressed in sr and the particle linear depolarization  $\delta$  in % along with the respective errors. References for each category are given in the right column. Measurements conducted in a field campaign are indicated with a number at the reference and explained in the footnote of the table, during a Polarstern or Meteor cruise with a bullet symbol ( $\bullet$ ), while the rest are from PollyNET/EARLINET stations. Measurements that were conducted with a non-TROPOS lidar, are accompanied with a star symbol (\*).

Aerosol type	$S_{355}$	$S_{532}$	$\delta_{355}$	$\delta_{532}$	Reference
Ash	$51 \pm 7.5$	$48 \pm 7.5$	$36 \pm 2.3$	-	Groß et al. (2012)*, Sicard et al. (2012), Kanitz (2012) $\bullet$
Saharan dust	$53.5 \pm 7.7$	$53.1 \pm 7.9$	$24.4 \pm 2.5$	$28 \pm 1.3$	Groß et al. (2011)* <sup>2</sup> , Preißler et al. (2011), Kanitz et al. (2013a) $\bullet$ , Baars et al. (2016), Rittmeister et al. (2017) $\bullet$ , Kaduk (2017) <sup>6</sup> , Haarig et al. (2017a) <sup>4</sup> , Urbanneck (2018) <sup>7</sup> , Bohlmann et al. (2018) $\bullet$ , Szczepanik et al. (2021), Haarig et al. (2022) <sup>4</sup>
Central Asian dust	$43.4 \pm 1.9$	$37.7 \pm 2.1$	$22.8 \pm 0.8$	$32.5 \pm 0.7$	Hofer et al. (2020) <sup>5</sup>
Middle Eastern dust	$39.5 \pm 6$	$37.4 \pm 5.3$	$24.2 \pm 2.3$	$28.4 \pm 1.6$	Müller et al. (2007) <sup>1</sup> , Kaduk (2017) <sup>6</sup> , Urbanneck (2018) <sup>7</sup> , Filioglou et al. (2020)
Smoke	$68.2 \pm 7.4$	$71.8 \pm 11.1$	$2.7 \pm 1.3$	$2.9 \pm 0.6$	Müller et al. (2007), Baars (2011) <sup>3</sup> , Tesche (2011) <sup>2</sup> , Pereira et al. (2014), Giannakaki et al. (2016) <sup>3</sup> , Janicka et al. (2016), Haarig et al. (2018), Floutsi et al. (2021) <sup>8</sup> , Ohneiser et al. (2021) <sup>9</sup> $\bullet$
Stratospheric smoke	$67.5 \pm 19.3$	$93.8 \pm 18.1$	$22.6 \pm 4$	$17.9 \pm 1.7$	Haarig et al. (2018), Ohneiser et al. (2020) <sup>8</sup>
Dust and smoke	$72.1 \pm 7.7$	$56.3 \pm 6.5$	$15.7 \pm 2$	$18.9 \pm 1.4$	Groß et al. (2011)* <sup>2</sup> , Tesche (2011) <sup>2</sup> , Kanitz et al. (2013a)* $\bullet$ , Giannakaki et al. (2016) <sup>3</sup> , Kanitz et al. (2014b) $\bullet$ , Kaduk (2017) <sup>6</sup> , Rittmeister et al. (2017) $\bullet$
Pollution	$51.1 \pm 8.7$	$47.4 \pm 7.4$	$1.1 \pm 0.3$	$2.8 \pm 1$	Ansmann et al. (2005), Müller et al. (2007), Tesche et al. (2007), Komppula et al. (2012) <sup>3</sup> , Preißler et al. (2013), Hänel et al. (2012) <sup>3</sup> , Giannakaki et al. (2016) <sup>3</sup> , Heese et al. (2017), Kaduk (2017) <sup>6</sup> , this study (Leipzig)
Dust and pollution	$48.5 \pm 9.2$	$46.4 \pm 8$	$15.7 \pm 1.7$	$17.7 \pm 2.5$	Leipzig, Germany*, Preißler et al. (2013), Janicka et al. (2016), Kaduk (2017) <sup>6</sup> , Rittmeister et al. (2017)
Dried marine	$28 \pm 6.6$	$26.9 \pm 10.6$	$7.5 \pm 1.7$	$8.3 \pm 1.1$	Haarig et al. (2017b) <sup>4</sup> , Bohlmann et al. (2018) $\bullet$
Clean marine	$22.4 \pm 5.6$	$21.9 \pm 13.4$	$1.3 \pm 0.3$	$1.4 \pm 0.3$	Groß et al. (2011)* <sup>2</sup> , Kaduk (2017) <sup>6</sup> , Bohlmann et al. (2018) $\bullet$ , Rittmeister et al. (2017) $\bullet$
Dust and marine	$39.4 \pm 5.6$	$32 \pm 7.8$	$14 \pm 1.5$	$14.7 \pm 1.1$	Groß et al. (2011)*, Kaduk (2017) <sup>6</sup> , Bohlmann et al. (2018) $\bullet$ , Rittmeister et al. (2017) $\bullet$
Central European background	$57 \pm 4.7$	$56.2 \pm 8.3$	$3.4 \pm 1.8$	$3.2 \pm 0.1$	Leipzig, Germany, Müller et al. (2007), this study (Leipzig)

<sup>1</sup>INDOEX, <sup>2</sup>SAMUM, <sup>3</sup>EUCAARI, <sup>4</sup>SALTRACE, <sup>5</sup>CADEX, <sup>6</sup>BACCHUS, <sup>7</sup>CyCARE/A-LIFE, <sup>8</sup>DACAPO-PESO, <sup>9</sup>MOSAic,



**Figure 1.** Locations of measurement campaigns (yellow stars) or permanent EARLINET stations (red/blue stars) from which data for the current study was used. Map source: primap.

Furthermore, the data collection is regularly updated aiming to provide a comprehensive up-to-date collection of the optical properties of the different aerosol types at the typical lidar wavelengths.

180 The portable TROPOS lidar systems BERTHA and Polly<sup>XT</sup> have been deployed at numerous campaigns, research platforms and locations (Fig. 1). In the following, a brief introduction of major field campaigns and research vessels, where TROPOS lidars operated, is presented. Measurements from the field campaigns listed below have contributed greatly to the collection presented here. Campaigns that contributed to the collection with a few measurements only are not listed here. In addition, the locations of all the campaigns relevant for this study and permanent measuring stations are indicated in Fig. 1.

### 185 2.2.1 Research cruises

Two German Research Vessels (RV), namely Meteor and Polarstern, serve as research platforms where Polly<sup>XT</sup> lidars have been deployed. The OCEANET-Atmosphere observatory, which includes a Polly<sup>XT</sup> lidar among other instruments, has been frequently operated aboard Polarstern for the transects from the Northern Hemisphere to the Southern Hemisphere and vice versa (e.g., Kanitz et al., 2013b; Bohlmann et al., 2018; Yin et al., 2019), as well as in the polar regions (e.g., Griesche  
190 et al., 2020; Engelmann et al., 2021). Pure marine aerosol conditions as well as complex mixtures, typically including sea-salt i.e., dust and marine aerosol mixtures, are being observed frequently. Data acquired during the transatlantic ship cruises and MOSAIC (more about that campaign in Sect. 2.2.9) have contributed greatly to the scientific efforts for aerosol monitoring,



**Table 2.** Extinction- ( $AE_{355/532}$ ) and backscatter-realized ( $AE_{b355/532}$  and  $AE_{b532/1064}$ ) Ångström exponents for the aerosol categories listed in Tab. 1.

Aerosol type	$AE_{355/532}$	$AE_{b355/532}$	$AE_{b532/1064}$
Ash	$0.8 \pm 0.6$	$0.6 \pm 0.4$	$1 \pm 0.4$
Saharan dust	$0.1 \pm 0.2$	$0.03 \pm 0.08$	$0.5 \pm 0.1$
Central Asian dust	$0.2 \pm 0.1$	$-0.2 \pm 0.03$	$0.4 \pm 0.01$
Middle Eastern dust	$0.1 \pm 0.1$	$0.4 \pm 0.2$	$0.7 \pm 0.2$
Smoke	$1.3 \pm 0.3$	$1.4 \pm 0.1$	$1.2 \pm 0.1$
Stratospheric smoke	$-0.3 \pm 0.4$	$1.2 \pm 0.4$	$1.2 \pm 0.6$
Dust and smoke	$1.4 \pm 0.2$	$0.5 \pm 0.1$	$1 \pm 0.05$
Pollution	$1.8 \pm 1.4$	$1.2 \pm 0.7$	$0.9 \pm 0.5$
Dust and pollution	$0.7 \pm 0.4$	$0.3 \pm 0.1$	$0.9 \pm 0.1$
Dried marine	$1.1 \pm 1.3$	$0.6 \pm 0.04$	$-0.07 \pm 0.07$
Clean marine	$0.7 \pm 1.3$	$0.8 \pm 0.1$	$0.5 \pm 0.1$
Dust and marine	$0.5 \pm 0.5$	$0.3 \pm 0.1$	$0.6 \pm 0.1$
Central European background	$1.5 \pm 0.2$	$1.4 \pm 0.2$	$1.2 \pm 0.2$

**Table 3.** Overview of RV cruises that are relevant for this study. The RV, cruise identification sequence and the corresponding study are indicated.

RV	Cruise ID	Reference
Polarstern	ANT-XXVI/1, ANT-XXVI/4 and ANT-XXVII/1	Kanitz et al. (2013a)
Polarstern	PS95 and PS98	Bohlmann et al. (2018)
Meteor	M96	Rittmeister et al. (2017)
Polarstern	MOSAIC20192020	Ohneiser et al. (2021)

by reaching places where no permanent stations can be established. Tab. 3 shows the identification sequences for the cruises relevant to this study.

### 195 2.2.2 SAMUM

The Saharan Mineral Dust Experiment (SAMUM) was focused on the investigation of the relationship between chemical composition, shape morphology, size distribution and optical effects of the dust particles originating from the Saharan desert (Ansmann et al., 2011). Two field campaigns were conducted in southern Morocco in 2006 and in Cape Verde in 2008 (SAMUM–1 and SAMUM–2, respectively). The combination of the ground-based multiwavelength Raman lidar BERTHA, two lidar sys-



200 tems from the University of Munich (the Portable Lidar System POLIS (Groß et al., 2008) and MULIS) and the airborne HSRL  
measurements (Falcon-20 research aircraft of the German Aerospace Center, DLR) allowed the profiling of pure dust optical  
properties as well as mixed aerosol plumes and provided a unique dataset that has been extensively used for radiation closure  
studies, development of appropriate dust parameterizations for large-scale and regional weather and climate models and in-situ  
comparison studies (Tesche et al., 2009a, b, 2011a, b).

### 205 **2.2.3 EUCAARI campaigns**

The European Integrated Project on Aerosol, Cloud, Climate, Air Quality Interactions project (EUCAARI; Kulmala et al.,  
2011) was a multidisciplinary project focused on the interactions between climate and air pollution. EUCAARI lasted for three  
years (01.01.2007–31.12.2010) and resulted in comprehensive datasets of aerosol properties from Europe and from four non-  
European countries (China, India, Brazil and South Africa). In the present study, measurements from all the aforementioned  
210 countries are included with a specific focus on measurements that were conducted in two EUCAARI campaigns in Amazonia  
and South Africa. A Polly<sup>XT</sup> lidar was deployed for the first time near Manaus, Brazil from January to November 2008. The  
long-term lidar observations obtained during that campaign have advanced our knowledge on the vertical aerosol distribution  
of Saharan dust, biomass-burning aerosol (BBA) and their mixtures, which get advected from Africa, and prevail the aerosol  
conditions of Amazonia (Baars, 2011). In addition, a clear distinction between the prevailing aerosol conditions during the  
215 wet (January – June) and dry season (July – November) was achieved (Baars, 2011). A Polly<sup>XT</sup> lidar was also operated in  
Elandsfontein, South Africa from 30 January 2010 to 31 January 2011. During that period biomass-burning aerosol from  
natural phenomena (lightning) and human-induced activities as well urban and industrial aerosol of anthropogenic origin  
were observed (Giannakaki et al., 2016). Measurements from the EUCAARI stations in China (Hänel et al., 2012) and India  
(Komppula et al., 2012) were heavily influenced by pollution-related aerosol. Complex mixtures of aged desert dust, biomass  
220 burning smoke and industrial pollution were frequently observed.

### **2.2.4 SALTRACE**

The Saharan Aerosol Long-range Transport and Aerosol-Cloud interaction Experiment (SALTRACE) was conducted from  
spring 2013 to summer 2014 at Barbados (Weinzierl et al., 2017). The campaign involved ground-based and airborne in-situ  
and remote-sensing observations. The main goal of SALTRACE was the characterization of Saharan dust particles after long-  
225 range transport (Groß et al., 2015; Haarig et al., 2017a) and its interaction with clouds (Haarig et al., 2019), as a follow-on to  
the SAMUM field campaign. TROPOS contributed with the deployment of the multiwavelength Raman lidar BERTHA (see  
Sect. 2) during the dusty summer conditions and the rather clear marine conditions in winter (Haarig et al., 2017a, b).

### **2.2.5 CADEX**

The Central Asian Dust Experiment (CADEX; Hofer et al., 2017, 2020) was focused on long-term observations of the op-  
230 tical and microphysical properties of Central Asian mineral dust. It was the first time that ground-based lidar observations



(performed with a Polly<sup>XT</sup> system at Dushanbe, Tajikistan) were conducted in Central Asia. CADEX lasted for two years (2014–2016, measurements conducted between 2015 and 2016) and resulted in major findings on optical properties of Central Asian dust, thus, establishing it as a separate aerosol type. In addition, the campaign pointed out the necessity of a permanent ground-based station in the area, which was later on established as part of EARLINET. It is obvious that campaigns aiming at  
235 monitoring a specific aerosol type, in a specific location where it is found in abundance, are very important in the global efforts of aerosol-type standardization.

### 2.2.6 BACCHUS

BACCHUS (Impact of Biogenic versus Anthropogenic emissions on Clouds and Climate: towards a Holistic UnderStanding) was an European collaborative project led by ETH Zurich (<https://www.bacchus-env.eu/>, last access: 18 October 2022). In the  
240 framework of BACCHUS, a Polly<sup>XT</sup> lidar system performed measurements in Nicosia, Cyprus in spring 2015. Pure aerosol types such as dust (Saharan and Middle Eastern), marine, and pollution as well as complex mixtures including smoke were regularly observed (Kaduk, 2017).

### 2.2.7 CyCARE and A-LIFE

The Cyprus Clouds Aerosol and Rain Experiment (CyCARE; Ansmann et al., 2019) took place at Limassol, Cyprus from  
245 October 2016 to March 2018 with main focus on the complex aerosol mixtures, vertical aerosol layering, and their influence on cloud evolution and precipitation processes. Polly<sup>XT</sup>, part of the LACROS (Leipzig Aerosol and Cloud Remote Observations System, the ground-based remote-sensing supersite of TROPOS; Bühl et al., 2013), was deployed at Limassol in 2017. During the deployment, the A-LIFE (Absorbing aerosol layers in a changing climate: aging, lifetime and dynamics) campaign took place (April 2017), which was led by the University of Vienna. A-LIFE aimed to investigate the properties of absorbing aerosol  
250 and in particular those of mineral dust, black carbon and their mixtures (<https://www.a-life.at/>, last access: 18 October 2022). In parallel to the A-LIFE campaign, the PRE-TECT campaign took place at the Greek atmospheric observatory of Finokalia in Crete, Greece. The campaign was led by the National Observatory of Athens (NOA) and aimed to improve the desert dust characterization from remote-sensing measurements. For that reason, the Polly<sup>XT</sup> lidar system of NOA was deployed at Finokalia.

### 255 2.2.8 DACAPO-PESO

The Dynamics, Aerosol, Clouds, And Precipitation Observations in the Pristine Environment of the Southern Ocean (DACAPO-PESO) field campaign took place in Punta Arenas, Chile and it was focused on the investigation of cloud formation and aerosol-cloud interaction in environments of contrasting aerosol conditions (Radenz et al., 2021a). LACROS (Bühl et al., 2013) was measuring continuously for a period of three years (2018–2021) and with respect to aerosol, significant lofted aerosol layers  
260 were observed occasionally in the troposphere of Punta Arenas (Floutsi et al., 2021). Furthermore, stratospheric smoke originating from the record-breaking Australian bushfires in January 2020 was fully captured by the lidar observations (Ohneiser



et al., 2020). However, the observations confirmed that in the general clean environment of Punta Arenas the aerosol backscatter is on average more than 30% below the mean of the backscatter observed in Europe (Limassol and Leipzig) (Radenz et al., 2021a). In addition, it was found that at Punta Arenas most aerosol is confined in the boundary layer with pristine conditions dominating aloft (Radenz et al., 2021a).

### 2.2.9 MOSAiC

During the MOSAiC (Multidisciplinary drifting Observatory for the Study of Arctic Climate) expedition, a Polly<sup>XT</sup> multi-wavelength polarization Raman lidar was operated onboard RV Polarstern from October 2019 to October 2020. For the first time, Polly<sup>XT</sup> conducted continuous measurements of aerosols and clouds (up to 30 km altitude) in the central Arctic (Engelmann et al., 2021). This unique dataset provided new insights about smoke trapped in the upper troposphere/lower stratosphere (UTLS) of the High Arctic in the winter of 2019–2020 (Ohneiser et al., 2021) and improved our knowledge on aerosol-cloud interactions (Engelmann et al., 2021).

### 2.2.10 EARLINET stations

Measurements from four permanent EARLINET stations have also significantly contributed to this study. The stations are mainly located in Europe: Leipzig (Germany), Évora (Portugal) and Warsaw (Poland). Pure aerosol types such as smoke, Saharan dust and pollution as well as their complex mixtures are frequently observed above the aforementioned stations. A non-European station located at Dushanbe (Tajikistan; see Sec. 2.2.5) was also considered.

## 3 DeLiAn

### 3.1 Intensive optical properties at 355 and 532 nm

Two intensive aerosol optical properties from the collection of ground-based observations described above (Sec. 2.2), namely the lidar ratio and the particle linear depolarization ratio at 355 nm, are contrasted against each other for several aerosol types and mixtures in Fig. 2. The aforementioned intensive properties exhibit the highest discriminatory power (e.g., as demonstrated in Burton et al., 2012). The dataset used for the conceptualization of the aerosol-typing-related activities of EarthCARE (Wandinger et al., 2016a; Illingworth et al., 2015) has been merged with the present dataset and is shown as semi-transparent symbols. Additionally to the intensive optical properties at 355 nm, in Fig. 3 we present the values for the same aerosol types at 532 nm. Furthermore, we show the wavelength dependence, i.e., the Ångström exponent contrasted to the lidar ratio and particle linear depolarization ratio, as presented in Fig. 4. Having the intensive properties at 355 and 532 nm allows not only the use of the spectral dependence for typing purposes, but also facilitates the bridging of datasets obtained at one of these wavelengths only as, e.g., in case of the spaceborne lidars CALIOP (532 nm) and ALADIN and ATLID (355 nm) or in the case of spaceborne and ground-based lidars (Amiridis et al., 2015).

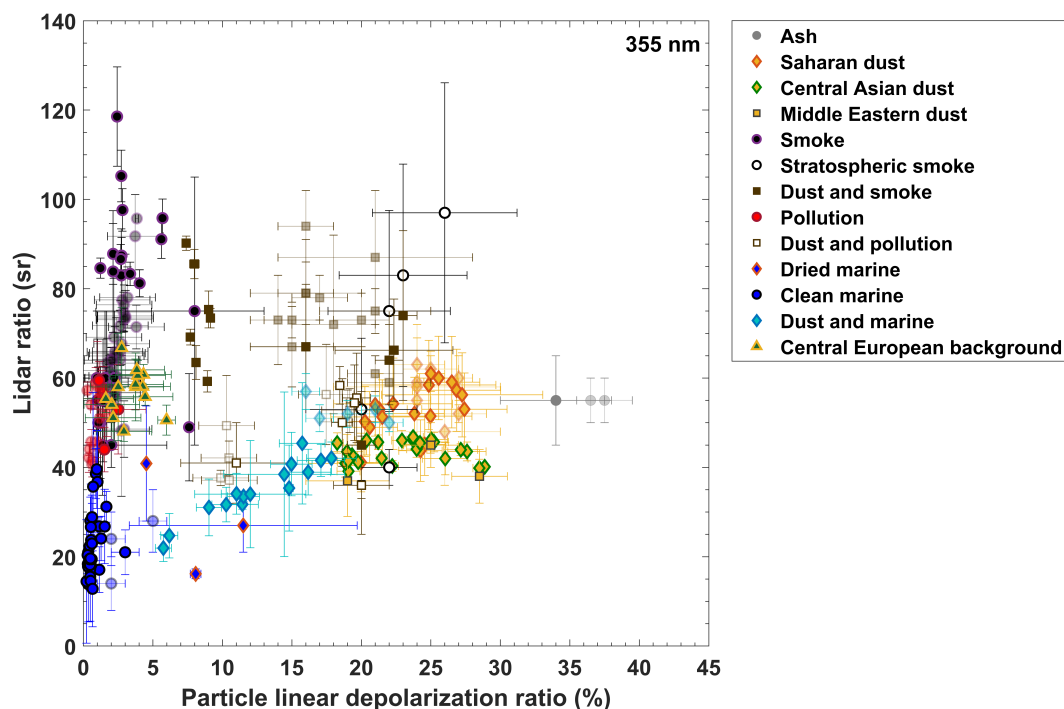


**Figure 2.** Intensive optical properties of different aerosol types, measured at 355 nm. The dataset used for the conceptualization of Earth-CARE's typing scheme is shown with faded markers.

### Ash

The volcanic ash category contains measurements of the Eyjafjallajökull eruption (April 2010) observed from various locations, including Maisach, Germany (faded grey circles in Fig. 2; Groß et al., 2012) with POLIS, near Bremerhaven, Germany conducted onboard the RV Polarstern (at 532 nm; Kanitz, 2012) and Évora, Portugal (no depolarization information available; Sicard et al., 2012). The mean lidar ratio and particle linear depolarization ratio at 355 and 532 nm and the mean Ångström exponents are reported in Tab. 1 and Tab. 2, respectively.

### Desert dust

Mineral dust is an important constituent of the atmospheric aerosol load, and in DeLiAn three aerosol categories have been dedicated for this specific aerosol type. Saharan dust has been targeted in many field campaigns and is the first of the three aforementioned categories (orange/red rhombuses in Fig. 2). Saharan dust is frequently advected above Europe, and observations over Portugal (Preißler et al., 2011), Warsaw (Szczepanik et al., 2021) and over Leipzig (Baars et al., 2016) have been included in the data collection. Long-range transported Saharan dust observed over Barbados during SALTRACE in 2013 and 2014 was also considered in the collection (Haarig et al., 2017a, 2022). The island of Cyprus, located in the eastern part

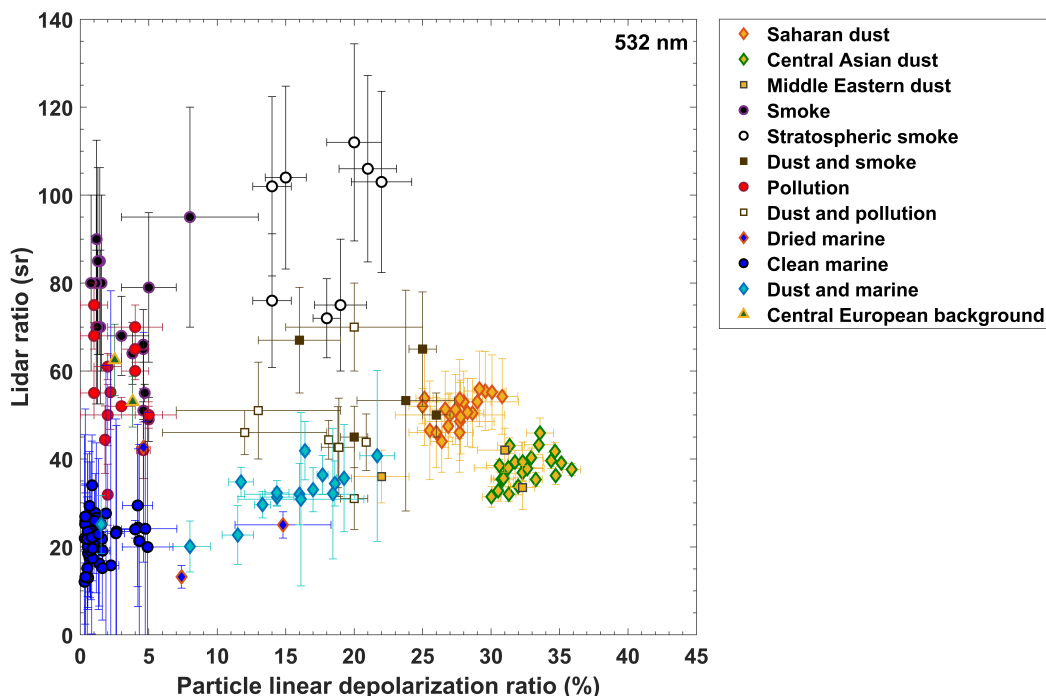


**Figure 3.** Intensive optical properties of different aerosol types, measured at 532 nm.

of the Mediterranean basin, is frequently affected by Saharan dust plumes and, therefore, dust measurements from Limassol  
305 (CyCARE/A-LIFE; Urbanneck, 2018) and from Nicosia (BACCHUS; Kaduk, 2017) were used. Saharan dust has also been  
observed from onboard the RV Polarstern, over the Atlantic Ocean (faded orange/red rhombuses in Fig. 2; Kanitz et al., 2013a)  
and near the Canary islands (Bohlmann et al., 2018), as well as from onboard the RV Meteor during a cruise from Guadeloupe  
to Cape Verde (Rittmeister et al., 2017). Measurements at 355 nm conducted with POLIS during the SAMUM-2 campaign  
at Cape Verde in 2008 were also considered (faded orange/red rhombuses in Fig. 2; Groß et al., 2011). At the current state  
310 of the experimental data collection, the representative mean lidar ratio and particle linear depolarization values at 355 nm  
are  $53.5 \pm 7.7$  sr and  $24.4 \pm 2.5\%$ , respectively. Optical information at wavelengths beyond EarthCARE's wavelength (i.e.,  
355 nm) are presented in Fig. 3 (532 nm) and the Ångström exponents are shown in Fig. 4. At 532 nm, the mean lidar ratio is  
 $53.1 \pm 7.9$  sr and the mean particle linear depolarization ratio is  $28 \pm 1.3\%$ . Mean values of the extinction-related Ångström  
exponent are  $0.1 \pm 0.2$  and the backscatter-related Ångström exponent values at both 355/532 and 532/1064 nm are around  
315  $0.03 \pm 0.08$  and  $0.5 \pm 0.1$ , respectively (Tab. 2 and Fig. 4).

In contrast to the findings from the major dust-targeting campaigns, SAMUM-1/2 and SALTRACE, in recent years it was  
confirmed that Central Asian dust has different optical properties than Saharan dust. Mineral dust that originates from the  
Central Asian deserts typically exhibits lower lidar ratio values (35–45 sr) than Saharan dust (50–60 sr), as shown by Hofer  
et al. (2017) on the basis of long-term observations in Tajikistan and, hence, has been introduced to DeLiAn as a separate

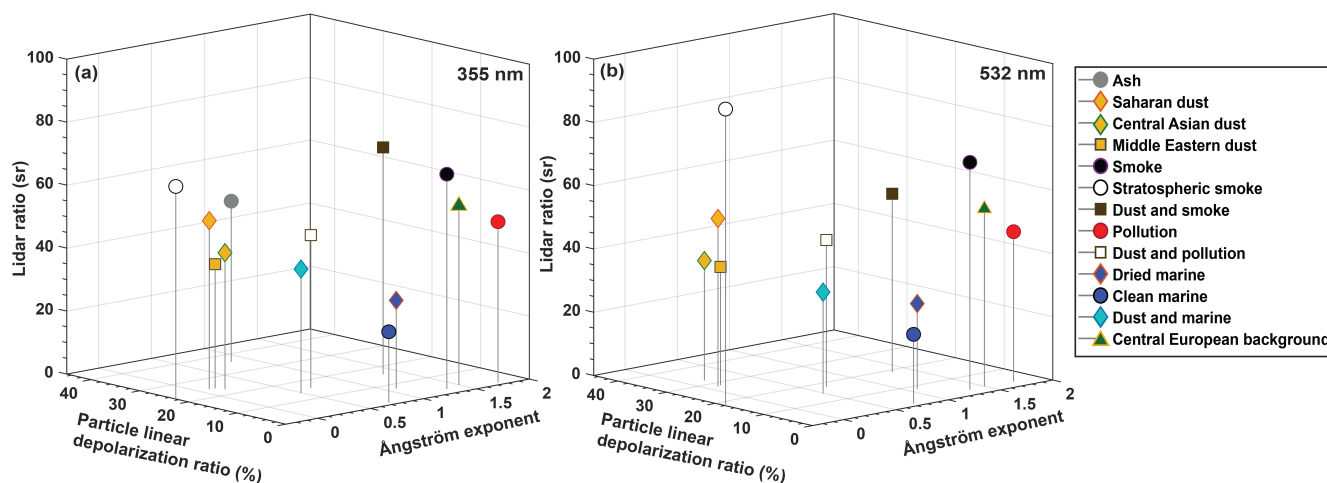


**Figure 4.** Mean lidar ratio and particle linear depolarization ratio at (a) 355 nm and (b) 532 nm versus the mean extinction-related Ångström exponent for the 13 aerosol categories.

320 aerosol type (green/yellow rhombuses in Fig. 2). The Central Asian dust measurements were conducted in the framework of  
 the CADEX field campaign at Dushanbe, Tajikistan (Hofer et al., 2017, 2020). Mean lidar ratio values for this aerosol category  
 are  $43.4 \pm 1.9$  and  $37.7 \pm 2.1$  sr at 355 and 532 nm, respectively. The mean particle linear depolarization ratios are  $22.8 \pm 0.8\%$   
 and  $32.5 \pm 0.7\%$  at 355 and 532 nm, respectively. Mean values of the extinction-related Ångström exponent are similar to those  
 of Saharan dust  $0.2 \pm 0.1$ , while the mean backscatter-related Ångström exponent values are  $-0.2 \pm 0.03\%$  and  $0.4 \pm 0.01\%$   
 325 at the wavelength pairs of 355/532 and 532/1064 nm, respectively.

Since the Eastern Mediterranean region has been characterized as a primary climate change “hot spot” (Lelieveld et al.,  
 2012), atmospheric measurements and campaigns have been intensified over the region. Complex mixtures of desert dust,  
 biomass-burning and pollution aerosol are usually encountered. Typically, dust particles observed above that region originate  
 either from the Sahara or the Middle Eastern deserts. Therefore, in addition to the Saharan and Central Asian Dust categories  
 330 we have introduced a new aerosol type: Middle Eastern dust. At the moment, this aerosol category (brown/yellow squares in  
 Fig. 2) comprises dust originating from Saudi Arabia (Müller et al., 2007) and observed within the framework of the Indian  
 Ocean Experiment (INDOEX; Ramanathan et al., 2001), from the United Arab Emirates (Filioglou et al., 2020) and mineral  
 dust measurements from Cyprus, specifically in Limassol (CyCARE/A-LIFE; Urbanneck, 2018) and in Nicosia (BACCHUS;  
 Kaduk, 2017). On average, the lidar ratios at 355 and 532 nm are  $39.5 \pm 6$  sr and  $37.4 \pm 5.3$  sr and the particle linear depolar-  
 335 ization ratios are  $24.2 \pm 2.3\%$  and  $28.4 \pm 1.6\%$ , respectively. The extinction- and backscatter-related Ångström exponents are  
 $0.1 \pm 0.1$ ,  $0.4 \pm 0.2$  (355/532 nm) and  $0.7 \pm 0.2$  (532/1064 nm), respectively.



## Smoke

The smoke category used for the conceptualization of EarthCARE's classification approach is based on measurements of smoke that were conducted during a EUCAARI campaign in the the Amazon Basin in 2008 (Baars et al., 2012). Measurements of  
340 lidar ratio and especially particle linear depolarization ratio at 355 nm were rare at the time of the campaign (depicted with faded black/purple circles in Fig. 2). Since then, 355 nm lidar measurements have become much more available and, therefore, smoke observations from other locations and fire types (e.g., smoldering or flaming combustion) have been observed too (depicted by black/purple circles in Fig. 2). Smoke observations from another EUCAARI campaign, this time from Elandsfontein, South Africa (Giannakaki et al., 2016) have been included in the data basis. Similarly, smoke measurements performed in the  
345 framework of SAMUM-2 at Cape Verde (Tesche, 2011) were added. Regional smoke and smoke from Australia was observed in the southern tip of South America (Punta Arenas, Chile) during the DACAPO-PESO field campaign (Floutsi et al., 2021). Smoke from Siberian wildfires, which was measured in the Arctic during the MOSAiC campaign, has also been added to the data collection (Ohneiser et al., 2021), which broadens even further the geographical coverage of the observations of that particular aerosol type. Smoke has been also observed above Europe frequently; from boreal forest fires in western Canada at  
350 Leipzig, Germany (Haarig et al., 2018), aged from Siberia/Canada measured at multiple EARLINET stations (Müller et al., 2007), long-range transported smoke from North America above Warsaw, Poland (Janicka et al., 2016, 2017) and fresh, locally-produced smoke above Portugal (Pereira et al., 2014). The 355 nm mean lidar ratio and particle linear depolarization ratio are  $68.2 \pm 7.4$  sr and  $2.7 \pm 1.3\%$ , respectively. At 532 nm, the mean smoke lidar ratio is  $71.8 \pm 11.1$  sr and, thus, higher and wider distributed compared to the 355 nm mean lidar ratio. The mean smoke particle linear depolarization ratio at the same wave-  
355 length is  $2.9 \pm 0.6\%$ . Extinction-related Ångström exponent values are on average around  $1.3 \pm 0.3$ , and backscatter-related Ångström exponent values are  $1.4 \pm 0.1$  and  $1.2 \pm 0.1$  for the wavelength pairs of 355/532 and 532/1064 nm.

## Stratospheric smoke

The different properties of smoke in the troposphere and in the stratosphere resulting from Pyrocumulonimbus convection were not realized before the intense Canadian wildfires of 2017 and were first studied by Haarig et al. (2018) and Ansmann  
360 et al. (2018) and the event's long-term evolution over Europe based on EARLINET measurements by Baars et al. (2019). In contrast to tropospheric smoke, stratospheric smoke is characterized by high depolarization ratios (at both 355 and 532 nm), a feature that was first observed in an elevated aged smoke layer in the upper troposphere, on the eastern seaboard of the United States, with an HSRL onboard the NASA B200 aircraft by Burton et al. (2015). In this data collection, the stratospheric smoke category (depicted by black/white circles in Fig. 2) includes the the aforementioned Canadian wildfires stratospheric smoke  
365 measurements (Haarig et al., 2018) and observations from the record-breaking Australian wildfires of January 2020 measured at Punta Arenas during DACAPO-PESO (Ohneiser et al., 2020). Mean lidar ratios for this aerosol category are  $67.5 \pm 19.3$  sr and  $93.8 \pm 18.1$  sr at 355 and 532 nm, respectively and, thus, significantly higher, on average, than for tropospheric smoke. Mean particle linear depolarization ratios are  $22.6 \pm 4\%$  and  $17.9 \pm 1.7\%$ . This is a significant finding, as aerosol particles in the stratosphere were usually attributed to volcanic origin (or e.g., generically classified as "stratospheric features" in the version



370 3 CALIPSO data; Kim et al., 2018). With these new findings it might be possible to distinguish stratospheric aerosol in more detail and new findings may resurface from historic datasets.

### Pollution

The pollution category includes measurements that have been conducted in cities of Europe, Asia and Africa. In particular, the category contains pollution measurements from multiple EARLINET stations in Europe (Müller et al., 2007), including  
375 the urban EARLINET station in Leipzig, from Évora (Preißler et al., 2013), from Nicosia (BACCHUS; Kaduk, 2017), from Elandsfontein (EUCAARI; Giannakaki et al., 2016), from China (more specifically at Xinken (Ansmann et al., 2005), at Beijing (Teschke et al., 2007), at Shangdianzi (Hänel et al., 2012) and at Guangzhou (in the framework of the German project “Megacities–Megachallenges – Informal Dynamics of Global Change”; Heese et al. (2017))) and from India (Gual Pahari- near New Dehli; Komppula et al., 2012). The mean 355-nm lidar ratio and particle linear depolarization ratio are  $51.1 \pm 8.7$  sr and  
380  $1.1 \pm 0.3\%$ , respectively. The corresponding properties for the 532 nm are  $47.4 \pm 7.4$  sr and  $2.8 \pm 1\%$ . Ångström exponents are reported in Tab. 2 and reflect the small size of the specific aerosol type.

### Marine

The clean marine category (depicted with blue/black circles in Fig. 2) contains measurements of marine particles (i.e., sea salt) that were conducted mostly onboard a RV or at a coastal station. Measurements conducted during two Polarstern cruises  
385 (PS95 from Bremerhaven, Germany to Cape Town, Republic of South Africa and PS98 from Punta Arenas to Bremerhaven; Bohlmann et al., 2018), during a Meteor cruise (M96 from Guadeloupe to Cape Verde; Rittmeister et al., 2017), at Nicosia, Cyprus (Kaduk, 2017) as well as at Cape Verde (faded blue/black circles in Fig. 2; SAMUM–2; Groß et al., 2011) have been included to the collection. At 355 nm the mean lidar ratio for this aerosol category is  $22.4 \pm 5.6$  sr, while the mean particle linear depolarization ratio is  $1.3 \pm 0.3\%$ . At 532 nm, the mean lidar ratio is  $21.9 \pm 13.4$  sr and the mean particle linear depolarization  
390 ratio is  $1.4 \pm 0.3\%$ , both indicating a very weak wavelength dependency. Ångström exponent values are on average  $0.7 \pm 1.3$  for the extinction-related,  $0.8 \pm 0.1$  and  $0.5 \pm 0.1$  for the backscatter-related (355/532 and 532/1064 nm, respectively).

Even though the optical properties of aerosol of marine origin do not show variability with respect to the source, when marine particles are exposed to dry atmospheric conditions, typically with relative humidity lower than 45%, they adopt a cubic-like shape due to the sodium chloride contained in the sea salt aerosol (Zieger et al., 2017). The cubic-like shape of the  
395 particles causes significantly higher particle linear depolarization ratios (Haarig et al., 2017b; Bohlmann et al., 2018). This fact was not realized earlier, e.g., in Illingworth et al. (2015) or in aerosol typing schemes such as the one of CALIPSO (Omar et al., 2005; Kim et al., 2018) and may have led to misclassification of this specific type, e.g., as mixture containing depolarizing mineral dust particles. Therefore, the introduction of the dried marine aerosol as a separate category was essential. The category includes measurements conducted at Barbados (2014) during SALTRACE (Haarig et al., 2017b), and above the Atlantic Ocean  
400 with RV Polarstern (Bohlmann et al., 2018) and are always observed on top of the local marine boundary layer. Measurements of dried marine particles are sparse, leading to only three measurements in this category. Therefore, the statistics presented here should be interpreted with caution. Dried marine particles exhibit on average lidar ratios of  $28 \pm 6.6$  sr and  $26.9 \pm 10.6$  sr



and particle linear depolarization ratios of  $7.5 \pm 1.7\%$  and  $8.3 \pm 1.1\%$  at 355 and 532 nm, respectively. The Ångström exponent values are presented in Tab. 2.

#### 405 **Central European background**

While optically similar to the pollution aerosol category, the “Central European background” aerosol type has been introduced to the collection, given the plethora of the permanent ground-based stations in the indicated geographical area and its resemblance to the more generalized aerosol category of clean continental in the CALIPSO typing scheme. The category (depicted with yellow/green triangles in Fig. 2) includes measurements of the background aerosol load in a typical Central European  
410 region (background aerosol measurements performed at Leipzig, and from multiple EARLINET stations, as adapted from Müller et al., 2007). Overall, this aerosol category exhibits slightly higher lidar ratios and particle linear depolarization ratios than pollution (Tab. 1 and 2).

#### **Mixtures**

Aerosol mixtures of dust particles with smoke, pollution and marine particles have been considered in DeLiAn. Dust and  
415 smoke mixtures from Cape Verde (SAMUM–2; Groß et al., 2011) and from measurements above the Atlantic ocean (RV Polarstern; Kanitz et al., 2013a) served as the starting point for the conceptualization of HETEAC (faded brown squares in Fig. 2). Additional measurements from Cape Verde (SAMUM–2; Tesche, 2011), from the Atlantic (conducted while onboard RV Polarstern, near Cape Verde and in the Caribbean; Kanitz et al. (2014b), and while onboard RV Meteor; Rittmeister et al. (2017)), in Elandsfontein (EUCAARI; Giannakaki et al., 2016) and in Nicosia (BACCHUS, Kaduk, 2017) were added to  
420 the data collection. The mean lidar ratio and particle linear depolarization ratio for dust-and-smoke mixtures at 355 nm are  $72.1 \pm 7.7$  sr and  $15.7 \pm 2\%$ , respectively. The same parameters for the newly-added 532-nm wavelength are  $56.3 \pm 6.5$  sr and  $18.9 \pm 1.4\%$ , respectively. Extinction- and backscatter-related Ångström exponents vary with wavelength, reflecting the versatile particle size range of the mixture (exact values in Tab. 2).

Mixtures of dust and marine particles (cyan/blue rhombuses in Fig. 2) are frequently observed in the lowermost atmosphere,  
425 especially in coastal stations such as in Cape Verde (faded cyan/blue rhombuses in Fig. 2; SAMUM–2; Groß et al., 2011) and in Nicosia, Cyprus (Kaduk, 2017). Dust and marine mixtures are also frequently observed with the RV Polarstern (Bohlmann et al., 2018) and RV Meteor (Rittmeister et al., 2017). The 355 nm mean lidar ratio and particle linear depolarization ratio are  $39.4 \pm 5.6$  sr and  $14 \pm 1.5\%$ , respectively. Accordingly,  $32 \pm 7.8$  sr and  $14.7 \pm 1.1\%$  for the 532 nm wavelength. The mean extinction-related Ångström exponent is  $0.5 \pm 0.5$  and mean backscatter-related Ångström exponents are  $0.3 \pm 0.1$  and  $0.6 \pm 0.1$   
430 for the wavelength pairs of 355/532 and 532/1064 nm, respectively.

Mixtures of dust and pollution (brown/white squares in Fig. 2) have been observed at Évora (Preißler et al., 2013), Warsaw (Janicka et al., 2016, 2017), Nicosia (Kaduk, 2017) and while onboard the RV Meteor above the Atlantic Ocean (Rittmeister et al., 2017). The mean lidar ratios for this category are  $48.5 \pm 9.2$  sr and  $46.4 \pm 8$  sr, and particle linear depolarization ratios are  $15.7 \pm 1.7\%$  and  $17.7 \pm 2.5\%$  at 355 and 532 nm, respectively. The mean extinction- and backscatter-related (355/532 and  
435 532/1064 nm) Ångström exponents are  $0.7 \pm 0.4$ ,  $0.3 \pm 0.1$  and  $0.9 \pm 0.1$ , respectively.



### 3.2 Statistical analysis of intensive optical properties

The main findings of this study are summarized in Fig. 4, which depicts the mean values of lidar ratio and particle linear depolarization ratio at (a) 355 nm and (b) 532 nm, respectively, against the mean extinction-related Ångström exponent for the different aerosol categories of Tab. 1. Incorporating the Ångström exponent as a third dimension results in more distinctive  
440 aerosol categories (in comparison to Fig. 2 and 3). For instance, the “Central European background” aerosol category can be now clearly distinguished from the pollution category as it exhibits higher extinction-related Ångström exponent values. The respective 2D plots, including the backscatter-related Ångström exponents are shown in Appendix A (Fig. A1 and A2).

A statistical analysis of the intensive optical properties was performed for the 13 different aerosol categories. It should be noted that since the data for each aerosol category have been collected from various sources (see Tab. 1), they naturally exhibit  
445 a variation in the number of data points per aerosol category. In addition, the measurements were performed by lidar systems with different capabilities and, therefore, not all intensive optical parameters were always available for all the observations (e.g., lidar ratio available only at one wavelength, or information on depolarization completely missing). Nevertheless, all available measurements were considered for the creation of DeLiAn and the statistical analysis presented here, and the number of data points used are listed in Tab. B1. The statistics for the lidar ratio and the particle linear depolarization ratio are presented in the  
450 form of boxplots, in Fig. 5 and Fig. 6 for the 355 nm and 532 nm wavelength, respectively. The statistics for all the Ångström exponents are presented in Fig. 7. The minimum and maximum values are indicated by the lower and upper whisker, while the median and mean values by the red lines and rhombuses, respectively. The lower part of each box indicates the 25% percentile and the upper part the 75% percentile. Red crosses represent the outliers (values greater than 1.5 times the interquartile range).

### 455 Comparison with CALIPSO aerosol subtypes

Statistics on the aerosol-type-separated optical properties can be used not only for the development of typing schemes, but can also consolidate already existing aerosol classification schemes, such as the typing scheme of CALIPSO (Omar et al., 2009; Kim et al., 2018). In Fig. 8, the lidar ratio (532 nm) assumed for the different aerosol types in the CALIPSO scheme is contrasted to the observations from the different ground-based lidars (Tab. 1). The CALIPSO lidar ratios for the different  
460 aerosol subtypes are adapted from Tab. 2 of Kim et al. (2018) (version 4). The version 4 stratospheric aerosol subtypes of “Polar stratospheric aerosol” and “Sulfate/other” are not included in the comparison, as there is no respective category in DeLiAn yet.

The assumptions of the lidar ratio of several aerosol subtypes appear to be in good agreement with the ground-based observations, e.g., for “Clean marine” and “Volcanic ash”, mainly due to an overlap in the data sources (Kim et al., 2018). Other aerosol subtype categories such as “Clean continental”, “Polluted dust”, “Elevated smoke” and “Dusty marine” agree well  
465 within the allowed variability, which is rather large for the CALIPSO data. The large variability of the assigned lidar ratio values to the aforementioned aerosol subtypes can potentially lead to large uncertainties in the retrieved extinction profiles. Kanitz et al. (2014a) had shown that for the version 3 CALIPSO data, the surface-dependent aerosol typing was not allowing for a correct classification of marine aerosol over land, and recently Ansmann et al. (2021) showed that stratospheric smoke

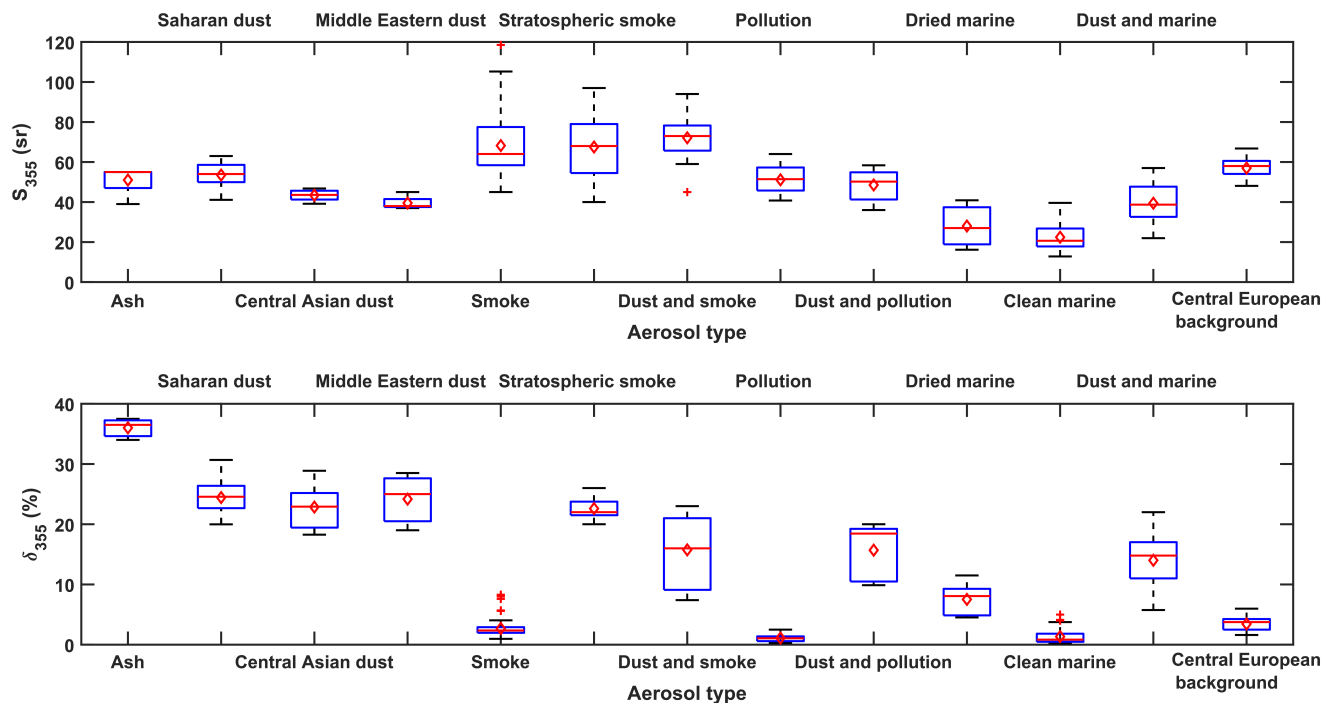


**Figure 5.** Statistics of the lidar ratio (top) and the particle linear depolarization ratio (bottom) at 355 nm for the 13 aerosol categories. The minimum and maximum values are indicated by the lower and upper whisker, median and mean values by the red lines and rhombuses, respectively. The lower part of each box indicates the 25% percentile and the upper part the 75% percentile. Red crosses represent the outliers.

layers are misclassified as sulfate aerosol layers (version 4 CALIPSO data). The present collection could be therefore utilized to reduce the aerosol-subtype-related variability linked to the 532 nm lidar ratio. Three CALIPSO subtypes namely “Dust”, “Polluted continental/smoke” and “Smoke” (stratospheric) seem to be problematic with respect to the present ground-based data collection. “Dust” has a lidar ratio of  $44 \pm 9$  sr, which is lower than what we observed for Saharan dust and higher than Central Asian and Middle Eastern dust. An increase of the lidar ratio variability of the specific aerosol subtype or a geographical-specific constraint would be therefore suggested to cover all the observations. The “Polluted continental/smoke” subtype has the highest variability and the nomenclature itself indicates that several aerosol types can be assigned under that category. With the current allowed variability, this category includes both the Smoke and Pollution categories of the present study, and is therefore correct. However, we would suggest the splitting of this subtype to allow a better discrimination in the radiative effects. Finally, the stratospheric smoke observations (see Tab. 1) suggest that the 532 nm lidar ratio of stratospheric smoke is higher than the one considered in the CALIPSO version 4 “Smoke” subtype (stratospheric).

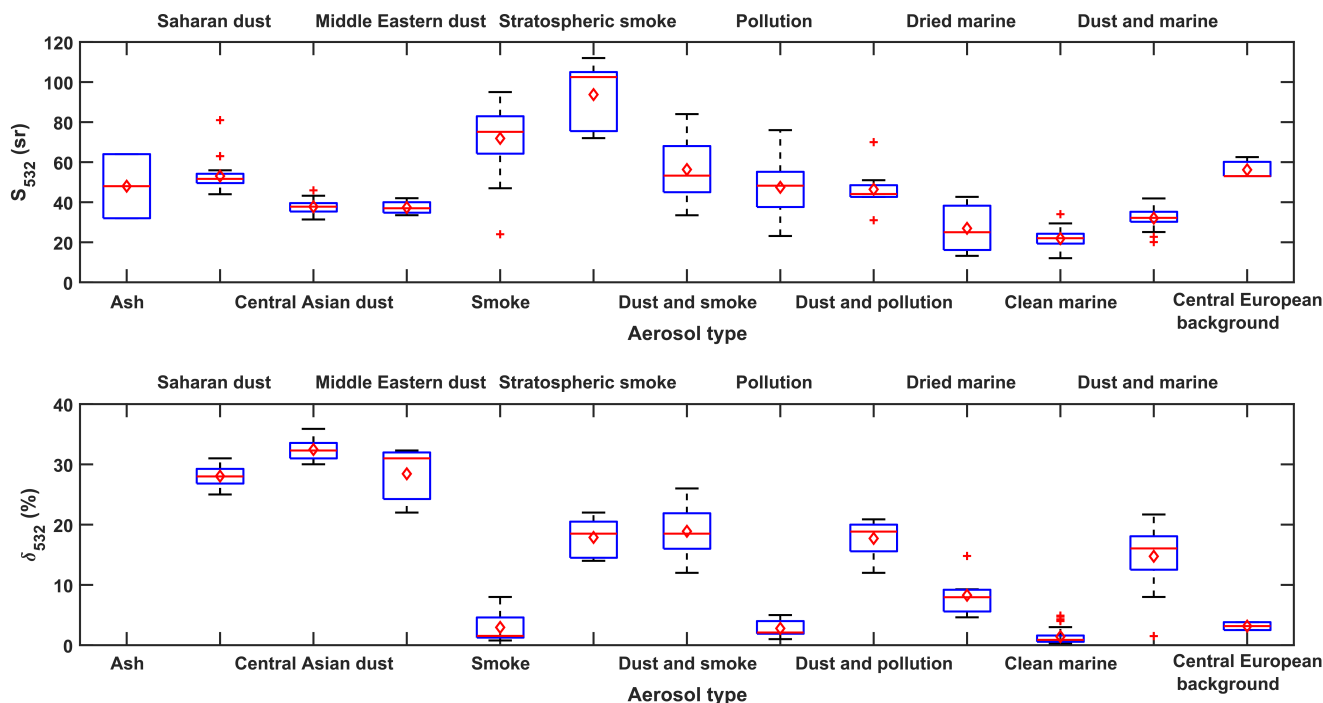
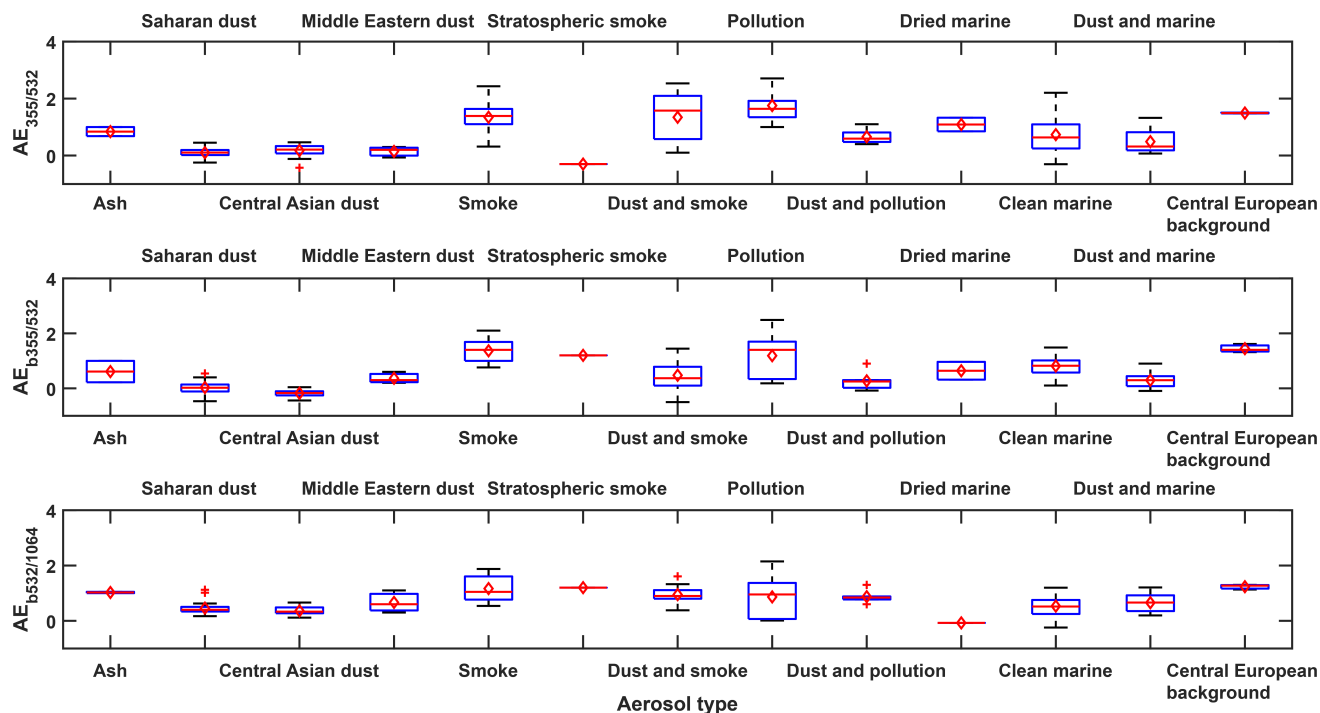


Figure 6. Same as in Fig. 5, but for 532 nm.

#### 480 4 Conclusions and outlook

A collection of intensive optical properties (DeLiAn) for various aerosol types based mainly on ground-based lidar observations was presented in this paper. DeLiAn merges measurements from old and more recent campaigns (large temporal coverage) and from various locations (large spatial coverage), and brings together aerosol types that were previously disregarded (e.g., dried marine particles, stratospheric smoke). The optical properties are presented at two wavelengths, 355 and 532 nm, and therefore, can be widely used for aerosol typing purposes, covering spaceborne lidars (CALIOP, ATLID) and ground-based lidar networks (e.g., MPLNET, EARLINET, AD-NET).

The presented statistics cover the most frequently observed aerosol types i.e., smoke, marine, pollution, dust and complex mixtures that they create as well as occasionally observed aerosol types e.g., dried marine particles. Such statistics can have multiple usages and are needed for aerosol classification purposes and aerosol typing schemes since they can be utilized as thresholds separating the different aerosol categories, or as a priori information. DeLiAn has been used for the development of both HETEAC (Wandinger et al., 2016a, Wandinger et al. in preparation) and HETEAC-Flex, a novel aerosol typing approach (Floutsi et al., 2019, Floutsi et al., in preparation), which shall homogenize aerosol typing from EarthCARE but also ground-based lidar systems with different capabilities and it will serve as a ground-based validation scheme for EarthCARE. The data collection of the different intensive optical properties can also be used for further improvement of already-existing aerosol



**Figure 7.** Statistics of the extinction-related (top), the 355/532 nm backscatter-related (middle) and the 532/1064 nm backscatter-related (bottom) Ångström exponents for the 13 aerosol categories.

495 classification schemes, for instance as shown in the case of CALIPSO, where more accurate lidar ratios can lead to better  
 extinction retrievals. Thus, DeLiAn could be considered by the MIRA (Models, In situ, and Remote sensing of Aerosols)  
 working group in their efforts for the creation of an updated CALIPSO lidar ratio climatology (version 5; Schuster et al.,  
 2022).

500 The presented data collection is only the beginning of a bigger effort for creating an aerosol climatology of intensive optical  
 properties based on ground-based lidar measurements. Measurements from other permanent PollyNET stations are planned to  
 be incorporated in DeLiAn to include geographical regions with interesting aerosol conditions which are currently underrepres-  
 ented. For instance, measurements from the Eastern Mediterranean region would significantly enrich many aerosol categories  
 such as marine, pollution, dust and their complex mixtures. Heese et al. (2022) recently presented a 2-year long lidar dataset  
 from the coastal city of Haifa, Israel. It was found that most of the observed aerosol layers were aerosol mixtures. Even though  
 505 a seasonal air-mass source attribution was performed by the authors using TRACE (Radenz et al., 2021b), a more detailed  
 case-by-case air-mass source attribution needs to be performed before the data are included to the data collection.

Data from recent measurement campaigns are also planned to be included in DeLiAn, after data collection and processing  
 is complete. Since the beginning of the ASKOS experiment (Amiridis and the ASKOS team, 2022) in the summer of 2021,  
 a Polly<sup>XT</sup> Raman lidar has been fully operational in Mindelo, Cape Verde. Clean marine, mineral dust as well as complex

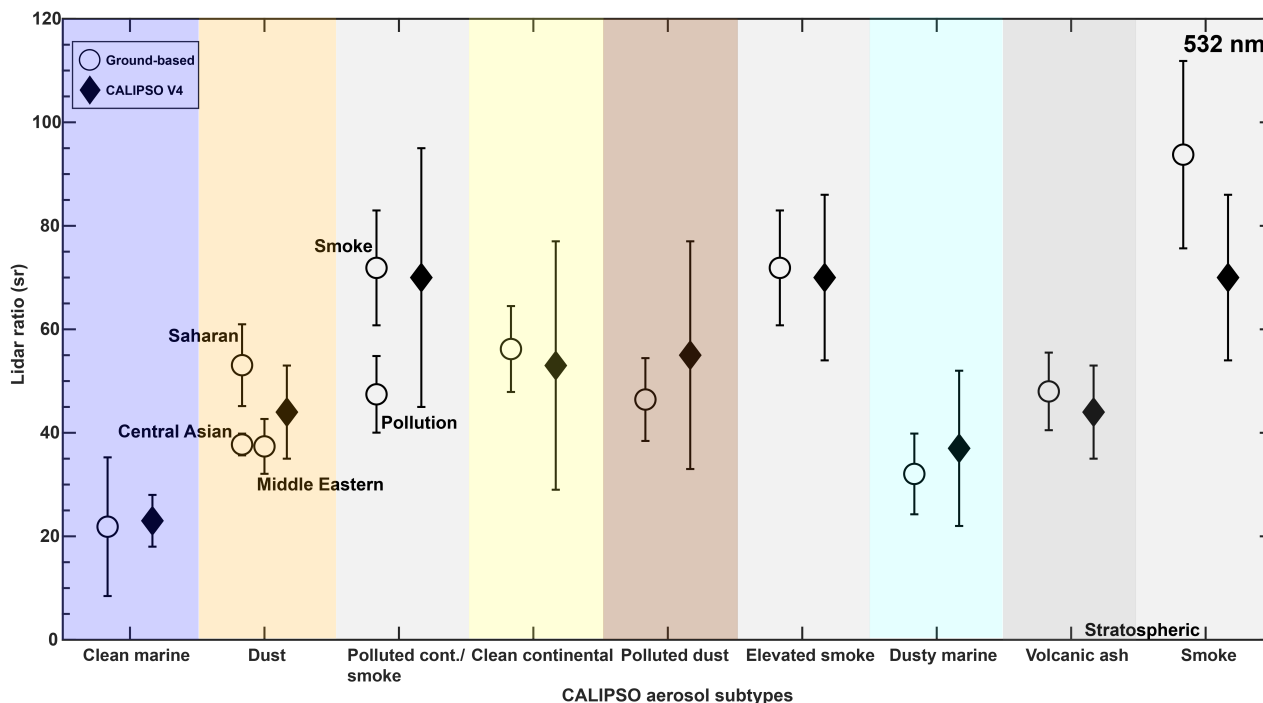


**Figure 8.** Comparison of the 532 nm lidar ratio as derived from ground-based lidars (white circles; this study) and from the CALIPSO aerosol subtypes (black rhombuses; Kim et al., 2018).

510 mixtures that they form have been observed regularly. Dried marine particles have also been observed often, typically on the top of the marine boundary layer.

In a recent study, Haarig et al. (2022) provided the first-ever lidar measurements of the lidar ratio and particle linear depolarization ratio for desert dust particles at all three lidar wavelengths (355, 532 and 1064 nm). As these measurements become more and more available, DeLiAn ought to be updated accordingly, since spectrally resolved information including  
515 the 1064 nm, is important for aerosol typing purposes.

*Data availability.* The data collection is planned to be published to Zenodo after the reviewing process is complete.



## Appendix A: 2D spaces of intensive optical properties

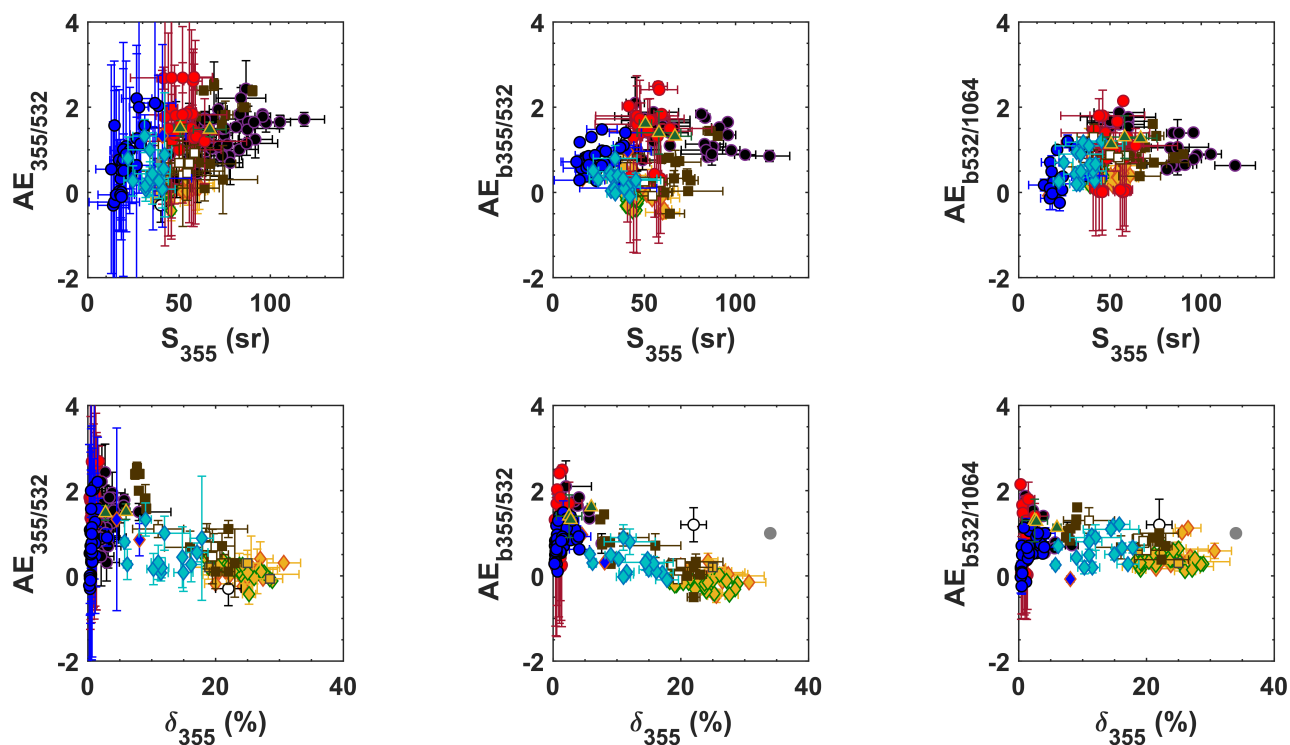


**Figure A1.** 355 nm lidar ratio ( $S$ ) and particle linear depolarization ratio ( $\delta$ ) against the extinction- ( $AE_{355/532}$ ) and backscatter-related ( $AE_{b355/532}$ ) Ångström exponent. The figure legend is the same as in Fig. 2.

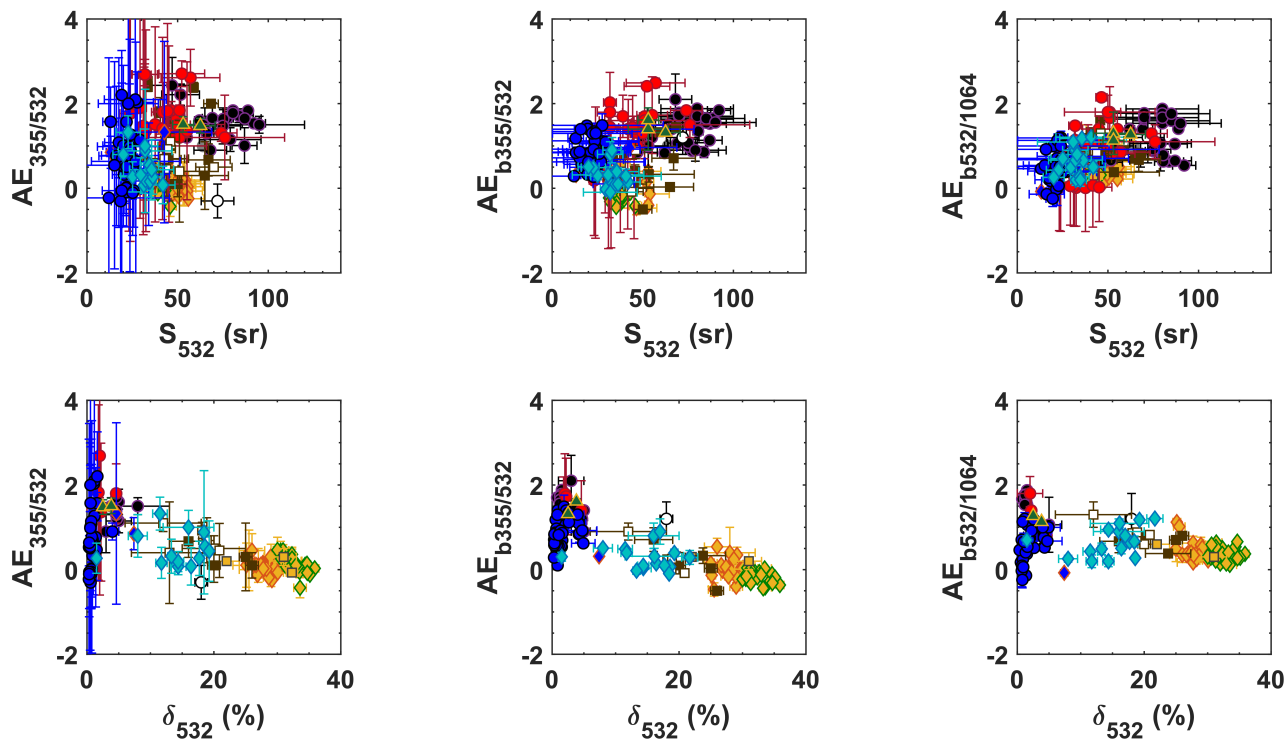


**Figure A2.** Same as Fig. A2, but for the 532 nm lidar ratio ( $S$ ) and particle linear depolarization ratio ( $\delta$ ).

### Appendix B: Number of data samples per aerosol category

The total number of samples per aerosol category and per intensive property that were considered for the statistics presented in  
520 Sec. 3.2 are shown in Tab. B1.



**Table B1.** Number of samples per aerosol category.

Aerosol type	Total	$S_{355}$	$\delta_{355}$	$S_{532}$	$\delta_{532}$	$AE_{355/532}$	$AE_{b355/532}$	$AE_{b532/1064}$
Ash	4	4	3	2	-	2	2	2
Saharan dust	30	29	27	26	29	22	19	19
Central Asian dust	23	23	23	23	23	23	23	23
Middle Eastern dust	4	4	3	4	3	3	3	3
Smoke	71	70	63	35	19	58	34	29
Stratospheric smoke	8	8	5	8	8	1	1	1
Dust and smoke	25	25	25	19	12	13	14	14
Pollution	42	26	20	42	16	25	27	27
Dust and pollution	15	15	13	8	8	8	6	6
Dried marine	7	3	7	3	7	2	2	1
Clean marine	52	38	52	48	49	33	48	30
Dust and marine	21	20	21	16	16	13	16	16
Central European background	14	14	14	3	2	2	3	3



*Author contributions.* The paper was conceptualized and written by AAF and HB. AAF collected, visualized the data and drafted the manuscript. UW provided guidance throughout the study. DA, JH and SFA were involved in the CADEX campaign, AA in the SAMUM-1 and -2 campaigns, PS, MR and BB in the DACAPO-PESO campaign, MH in SALTRACE campaign, and HB, EG and MK in the EUCAARI campaign. MH and REM were involved in the CyCARE and A-LIFE campaigns, EM and VA in the BACCHUS, CyCARE, A-LIFE and PRE-TECT campaigns, AG in the A-LIFE and PRE-TECT campaigns. MF and MK were responsible for the lidar observations in the United Arab Emirates. TK, SB, KO and MR were involved in Polarstern cruises. Instruments onboard Polarstern have been regularly taken care of by RE, HB and ZY. ISS, LJ, DB and HB are responsible for the PollyNET/EARLINET stations mentioned in this study. DA, BH, AS and RE have continuously contributed to the development and upgrade of Polly<sup>XT</sup> lidar systems.

*Competing interests.* UW and VA are members of the editorial board of Atmospheric Measurement Techniques. The authors have no further conflict of interest to declare.

*Acknowledgements.* The authors acknowledge support through the following projects and research programs:

- ACTRIS under grant agreement no. 262 254 of the European Union Seventh Framework Programme (FP7/2007–2013)
- ACTRIS-2 under grant agreement no. 654109 from the European Union’s Horizon 2020 research and innovation programme
- EUCAARI funded by the European Union Sixth Framework Programme (FP6) under grant no. 036 833-2
- CADEX funded by the German Federal Ministry of Education and Research (BMBF) under the grant no. 01DK14014
- the Gottfried Wilhelm Leibniz Association (OCEANET project in the framework of PAKT)
- BEYOND (funded under: FP7-REGPOT-2012-2013-1) under grant agreement no. 316210.
- “Megacities-Megachallenge – Informal Dynamics of Global Change” (SPP 1233) funded by the German Research Foundation (DFG)
- Foundation of Science and Technology of Poland (FNiTP) Grant no. 519/FNiTP/115/2010
- National Science Centre of Poland (NCN, DAINA-2) Grant no. 2020/38/L/ST10/00480
- Polarstern expeditions ANT-XXVI/1, ANT-XXVI/4, ANT-XXVII/1, AWI\_PS75\_00, AWI\_PS77\_00, AWI\_PS81\_00, AWI\_PS83\_00, AWI\_PS95\_00, AWI\_PS98\_00, AWI\_PS122\_00 and MOSAiC20192020
- SAMUM funded by the Deutsche Forschungsgemeinschaft (DFG) under grant number FOR 539.
- BACCHUS funded by the European Union’s 7th Framework Programme (FP7/2007-2013) under grant agreement no. 603445.
- A-LIFE funded by the European Research Council (grant no. 640458).
- EVAA funded by the German Federal Ministry for Economic Affairs and Energy (BMWi) under grant no. 50EE1721C.
- European Research Council (ERC) under the European Community’s Horizon 2020 research and innovation framework programme — ERC grant agreement no. 725698 (D-TECT)
- PANhellenic Geophysical Observatory of Antikythera (PANGEA) of the National Observatory of Athens, Greece



- 550 – "EXCELSIOR": ERATOSTHENES: EXcellence Research Centre for Earth Surveillance and Space-Based Monitoring of the Environment H2020 Widespread Teaming project ([www.excelsior2020.eu](http://www.excelsior2020.eu)), funded from the European Union's Horizon 2020 research and innovation programme under Grant Agreement No. 857510, from the Government of the Republic of Cyprus through the Directorate General for the European Programmes, Coordination and Development and the Cyprus University of Technology
- PoLiCyTa project: PollyXT-CYP funded by the German Federal Ministry of Education and Research (BMBF)
- 555 – The National Fund for Scientific and Technological Development of Chile, FONDECYT, through grant agreement No. 11181335.

Furthermore, the authors would like to acknowledge and thank all the scientists and technical personnel involved in the realisation of all the measurement campaigns and maintenance of the lidar stations, the RV Meteor team for their support during the M96 cruise, the Alfred Wegener Institute and the RV Polarstern crew during the ship cruises. Many improvements, both, in terms of hard and software were triggered by the fruitful discussions and network activities within EARLINET and ACTRIS.



## 560 References

- Althausen, D., Müller, D., Ansmann, A., Wandinger, U., Hube, H., Clauer, E., and Zörner, S.: Scanning 6-Wavelength 11-Channel Aerosol Lidar, *J. Atmos. Ocean. Tech.*, 17, 1469–1482, [https://doi.org/10.1175/1520-0426\(2000\)017<1469:SWCAL>2.0.CO;2](https://doi.org/10.1175/1520-0426(2000)017<1469:SWCAL>2.0.CO;2), 2000.
- Althausen, D., Engelmann, R., Baars, H., Heese, B., Ansmann, A., Müller, D., and Komppula, M.: Portable Raman Lidar Polly(XT) for Automated Profiling of Aerosol Backscatter, Extinction, and Depolarization, *J. Atmos. Ocean. Tech.*, 26, 2366–2378, <https://doi.org/10.1175/2009jtech1304.1>, 2009.
- 565 Amiridis, V. and the ASKOS team: The ASKOS experiment for desert dust science applications, EGU General Assembly, <https://doi.org/10.5194/egusphere-egu22-3633>, 2022.
- Amiridis, V., Marinou, E., Tsekeri, A., Wandinger, U., Schwarz, A., Giannakaki, E., Mamouri, R., Kokkalis, P., Biniotoglou, I., Solomos, S., Herekakis, T., Kazadzis, S., Gerasopoulos, E., Proestakis, E., Kottas, M., Balis, D., Papayannis, A., Kontoes, C., Kourtidis, K., Pappagiannopoulos, N., Mona, L., Pappalardo, G., Le Rille, O., and Ansmann, A.: LIVAS: a 3-D multi-wavelength aerosol/cloud database based on CALIPSO and EARLINET, *Atmos. Chem. Phys.*, 15, 7127–7153, <https://doi.org/10.5194/acp-15-7127-2015>, 2015.
- 570 Ansmann, A. and Müller, D.: Lidar and Atmospheric Aerosol Particles, in: *Lidar: Range-Resolved Optical Remote Sensing of the Atmosphere*, edited by Weitkamp, C., vol. 102 of *Springer Series in Optical Sciences*, pp. 105–141, Springer, New York, New York, USA, 1 edn., 2005.
- 575 Ansmann, A., Wandinger, U., Riebesell, M., Weitkamp, C., and Michaelis, W.: Independent measurement of extinction and backscatter profiles in cirrus clouds by using a combined Raman elastic-backscatter lidar, *Appl. Opt.*, 31, 7113–7131, <https://doi.org/10.1364/AO.31.007113>, 1992.
- Ansmann, A., Althausen, D., Wandinger, U., Franke, K., Müller, D., Wagner, F., and Heintzenberg, J.: Vertical profiling of the Indian aerosol plume with six-wavelength lidar during INDOEX: A first case study, *Geophysical Research Letters*, 27, 963–966, <https://doi.org/https://doi.org/10.1029/1999GL010902>, 2000.
- 580 Ansmann, A., Wagner, F., Müller, D., Althausen, D., Herber, A., von Hoyningen-Huene, W., and Wandinger, U.: European pollution outbreaks during ACE 2: Optical particle properties inferred from multiwavelength lidar and star-Sun photometry, *J. Geophys. Res.-Atmos.*, 107, AAC 8–1–AAC 8–14, <https://doi.org/10.1029/2001JD001109>, 2002.
- Ansmann, A., Engelmann, R., Althausen, D., Wandinger, U., Hu, M., Zhang, Y. H., and He, Q. S.: High aerosol load over the Pearl River Delta, China, observed with Raman lidar and Sun photometer, *Geophys. Res. Lett.*, 32, 4, <https://doi.org/10.1029/2005gl023094>, 2005.
- 585 Ansmann, A., Petzold, A., Kandler, K., Tegen, I., Wendisch, M., Müller, D., Weinzierl, B., Müller, T., and Heintzenberg, J.: Saharan Mineral Dust Experiments SAMUM–1 and SAMUM–2: what have we learned?, *Tellus B*, 63, 403–429, <https://doi.org/10.1111/j.1600-0889.2011.00555.x>, 2011.
- Ansmann, A., Baars, H., Chudnovsky, A., Mattis, I., Veselovskii, I., Haarig, M., Seifert, P., Engelmann, R., and Wandinger, U.: Extreme levels of Canadian wildfire smoke in the stratosphere over central Europe on 21–22 August 2017, *Atmos. Chem. Phys.*, 18, 11 831–11 845, <https://doi.org/10.5194/acp-18-11831-2018>, 2018.
- 590 Ansmann, A., Mamouri, R. E., Bühl, J., Seifert, P., Engelmann, R., Hofer, J., Nisantzi, A., Atkinson, J. D., Kanji, Z. A., Sierau, B., Vrekoussis, M., and Sciare, J.: Ice-nucleating particle versus ice crystal number concentration in altocumulus and cirrus layers embedded in Saharan dust: a closure study, *Atmos. Chem. Phys.*, 19, 15 087–15 115, <https://doi.org/10.5194/acp-19-15087-2019>, 2019.
- 595 Ansmann, A., Ohneiser, K., Chudnovsky, A., Baars, H., and Engelmann, R.: CALIPSO Aerosol-Typing Scheme Misclassified Stratospheric Fire Smoke: Case Study From the 2019 Siberian Wildfire Season, *Front. Env. Sc.*, 9, <https://doi.org/10.3389/fenvs.2021.769852>, 2021.



- Antuña-Marrero, J. C., Landulfo, E., Estevan, R., Barja, B., Robock, A., Wolfram, E., Ristori, P., Clemesha, B., Zaratti, F., Forno, R., Armandillo, E., Bastidas, E., de Frutos Baraja, M., Whiteman, D. N., Quel, E., Barbosa, H. M. J., Lopes, F., Montilla-Rosero, E., and Guerrero-Rascado, J. L.: LALINET: The First Latin American–Born Regional Atmospheric Observational Network, *B. Am. Meteorol. Soc.*, 98, 1255–1275, <https://doi.org/10.1175/BAMS-D-15-00228.1>, 2017.
- 600 Baars, H.: Aerosol profiling with lidar in the Amazon Basin during wet and dry season, PhD dissertation, Leipzig University, <https://nbn-resolving.org/urn:nbn:de:bsz:15-qucosa-98757>, 2011.
- Baars, H. and Yin, Z.: PollyNET/Pollynet\_Processing\_Chain: Version 2.0, <https://doi.org/10.5281/zenodo.3774689>, 2020.
- Baars, H., Ansmann, A., Engelmann, R., and Althausen, D.: Continuous monitoring of the boundary-layer top with lidar, *Atmos. Chem. Phys.*, 8, 7281–7296, <https://doi.org/10.5194/acp-8-7281-2008>, 2008.
- 605 Baars, H., Ansmann, A., Althausen, D., Engelmann, R., Heese, B., Müller, D., Artaxo, P., Paixao, M., Pauliquevis, T., and Souza, R.: Aerosol profiling with lidar in the Amazon Basin during the wet and dry season, *J. Geophys. Res.-Atmos.*, 117, 16, <https://doi.org/10.1029/2012jd018338>, 2012.
- Baars, H., Kanitz, T., Engelmann, R., Althausen, D., Heese, B., Komppula, M., Preissler, J., Tesche, M., Ansmann, A., Wandinger, U., Lim, J. H., Ahn, J. Y., Stachlewska, I. S., Amiridis, V., Marinou, E., Seifert, P., Hofer, J., Skupin, A., Schneider, F., Bohlmann, S., Foth, A., Bley, S., Pfuller, A., Giannakaki, E., Lihavainen, H., Viisanen, Y., Hooda, R. K., Pereira, S. N., Bortoli, D., Wagner, F., Mattis, I., Janicka, L., Markowicz, K. M., Achtert, P., Artaxo, P., Pauliquevis, T., Souza, R. A. F., Sharma, V. P., van Zyl, P. G., Beukes, J. P., Sun, J. Y., Rohwer, E. G., Deng, R. R., Mamouri, R. E., and Zamorano, F.: An overview of the first decade of Polly(NET): an emerging network of automated Raman-polarization lidars for continuous aerosol profiling, *Atmos. Chem. Phys.*, 16, 5111–5137, [https://doi.org/10.5194/acp-](https://doi.org/10.5194/acp-16-5111-2016)
- 610 16-5111-2016, 2016.
- Baars, H., Ansmann, A., Ohneiser, K., Haarig, M., Engelmann, R., Althausen, D., Hanssen, I., Gausa, M., Pietruczuk, A., Szkop, A., Stachlewska, I. S., Wang, D., Reichardt, J., Skupin, A., Mattis, I., Trickl, T., Vogelmann, H., Navas-Guzmán, F., Haeefe, A., Acheson, K., Ruth, A. A., Tatarov, B., Müller, D., Hu, Q., Podvin, T., Goloub, P., Veselovskii, I., Pietras, C., Haeffelin, M., Fréville, P., Sicard, M., Comerón, A., Fernández García, A. J., Molero Menéndez, F., Córdoba-Jabonero, C., Guerrero-Rascado, J. L., Alados-Arboledas, L., Bortoli, D., Costa, M. J., Dionisi, D., Liberti, G. L., Wang, X., Sannino, A., Papagiannopoulos, N., Boselli, A., Mona, L., D’Amico, G., Romano, S., Perrone, M. R., Belegante, L., Nicolae, D., Grigorov, I., Gialitaki, A., Amiridis, V., Soupiona, O., Papayannis, A., Mamouri, R. E., Nisantzi, A., Heese, B., Hofer, J., Schechner, Y. Y., Wandinger, U., and Pappalardo, G.: The unprecedented 2017–2018 stratospheric smoke event: decay phase and aerosol properties observed with the EARLINET, *Atmos. Chem. Phys.*, 19, 15 183–15 198, [https://doi.org/10.5194/acp-](https://doi.org/10.5194/acp-19-15183-2019)
- 620 19-15183-2019, 2019.
- Baars, H., Radenz, M., Floutsi, A. A., Engelmann, R., Althausen, D., Heese, B., Ansmann, A., Flament, T., Dabas, A., Trajon, D., Reitebuch, O., Bley, S., and Wandinger, U.: Californian Wildfire Smoke Over Europe: A First Example of the Aerosol Observing Capabilities of Aeolus Compared to Ground-Based Lidar, *Geophys. Res. Lett.*, 48, <https://doi.org/10.1029/2020GL092194>, 2021.
- Belegante, L., Bravo-Aranda, J. A., Freudenthaler, V., Nicolae, D., Nemuc, A., Ene, D., Alados-Arboledas, L., Amodeo, A., Pappalardo, G., D’Amico, G., Amato, F., Engelmann, R., Baars, H., Wandinger, U., Papayannis, A., Kokkalis, P., and Pereira, S. N.: Experimental techniques for the calibration of lidar depolarization channels in EARLINET, *Atmos. Meas. Tech.*, 11, 1119–1141, <https://doi.org/10.5194/amt-11-1119-2018>, 2018.
- 630 Bohlmann, S., Baars, H., Radenz, M., Engelmann, R., and Macke, A.: Ship-borne aerosol profiling with lidar over the Atlantic Ocean: from pure marine conditions to complex dust-smoke mixtures, *Atmos. Chem. Phys.*, 18, 9661–9679, <https://doi.org/10.5194/acp-18-9661-2018>, 2018.



- 635 Boucher, O., Randall, D., Artaxo, P., Bretherton, C., Feingold, G., Forster, P., Kerminen, V.-M., Kondo, Y., Liao, H., and Lohmann, U.: Clouds and aerosols, in: *Climate change 2013: the physical science basis. Contribution of Working Group I to the Fifth Assessment Report of the Intergovernmental Panel on Climate Change*, pp. 571–657, Cambridge University Press, Cambridge, United Kingdom and New York, NY, USA, [https://www.ipcc.ch/site/assets/uploads/2018/02/WG1AR5\\_Chapter07\\_FINAL-1.pdf](https://www.ipcc.ch/site/assets/uploads/2018/02/WG1AR5_Chapter07_FINAL-1.pdf), (last access: 18 October 2022), 2013.
- Bravo-Aranda, J. A., Belegante, L., Freudenthaler, V., Alados-Arboledas, L., Nicolae, D., Granados-Muñoz, M. J., Guerrero-Rascado, J. L.,  
640 Amodeo, A., D’Amico, G., Engelmann, R., Pappalardo, G., Kokkalis, P., Mamouri, R., Papayannis, A., Navas-Guzmán, F., Olmo, F. J., Wandinger, U., Amato, F., and Haeffelin, M.: Assessment of lidar depolarization uncertainty by means of a polarimetric lidar simulator, *Atmos. Meas. Tech.*, 9, 4935–4953, <https://doi.org/10.5194/amt-9-4935-2016>, 2016.
- Burton, S. P., Ferrare, R. A., Hostetler, C. A., Hair, J. W., Rogers, R. R., Obland, M. D., Butler, C. F., Cook, A. L., Harper, D. B., and Froyd, K. D.: Aerosol classification using airborne High Spectral Resolution Lidar measurements - methodology and examples, *Atmos. Meas. Tech.*, 5, 73–98, <https://doi.org/10.5194/amt-5-73-2012>, 2012.  
645
- Burton, S. P., Hair, J. W., Kahnert, M., Ferrare, R. A., Hostetler, C. A., Cook, A. L., Harper, D. B., Berkoff, T. A., Seaman, S. T., Collins, J. E., Fenn, M. A., and Rogers, R. R.: Observations of the spectral dependence of linear particle depolarization ratio of aerosols using NASA Langley airborne High Spectral Resolution Lidar, *Atmos. Chem. Phys.*, 15, 13 453–13 473, <https://doi.org/10.5194/acp-15-13453-2015>, 2015.
- 650 Bühl, J., Seifert, P., Wandinger, U., Baars, H., Kanitz, T., Schmidt, J., Myagkov, A., Engelmann, R., Skupin, A., Heese, B., Klepel, A., Althausen, D., and Ansmann, A.: LACROS: the Leipzig Aerosol and Cloud Remote Observations System, vol. 8890 of *SPIE Remote Sensing*, SPIE, 10.1117/12.2030911, 2013.
- D’Amico, G., Amodeo, A., Baars, H., Binietoglou, I., Freudenthaler, V., Mattis, I., Wandinger, U., and Pappalardo, G.: EARLINET Single Calculus Chain - overview on methodology and strategy, *Atmos. Meas. Tech.*, 8, 4891–4916, <https://doi.org/10.5194/amt-8-4891-2015>,  
655 2015.
- do Carmo, J. P., de Villele, G., Wallace, K., Lefebvre, A., Ghose, K., Kanitz, T., Chassat, F., Corselle, B., Belhadj, T., and Bravetti, P.: Atmospheric LIDAR (ATLID): Pre-Launch Testing and Calibration of the European Space Agency Instrument That Will Measure Aerosols and Thin Clouds in the Atmosphere, *Atmosphere*, 12, 76, <https://doi.org/10.3390/atmos12010076>, 2021.
- Engelmann, R., Kanitz, T., Baars, H., Heese, B., Althausen, D., Skupin, A., Wandinger, U., Komppula, M., Stachlewska, I. S., Amiridis, V.,  
660 Marinou, E., Mattis, I., Linne, H., and Ansmann, A.: The automated multiwavelength Raman polarization and water-vapor lidar Polly<sup>XT</sup>: the neXT generation, *Atmos. Meas. Tech.*, 9, 1767–1784, <https://doi.org/10.5194/amt-9-1767-2016>, 2016.
- Engelmann, R., Ansmann, A., Ohneiser, K., Griesche, H., Radenz, M., Hofer, J., Althausen, D., Dahlke, S., Maturilli, M., Veselovskii, I., Jimenez, C., Wiesen, R., Baars, H., Bühl, J., Gebauer, H., Haarig, M., Seifert, P., Wandinger, U., and Macke, A.: Wildfire smoke, Arctic haze, and aerosol effects on mixed-phase and cirrus clouds over the North Pole region during MOSAiC: an introduction, *Atmos. Chem. Phys.*, 21, 13 397–13 423, <https://doi.org/10.5194/acp-21-13397-2021>, 2021.  
665
- Filioglou, M., Giannakaki, E., Backman, J., Kesti, J., Hirsikko, A., Engelmann, R., O’Connor, E., Leskinen, J. T. T., Shang, X., Korhonen, H., Lihavainen, H., Romakkaniemi, S., and Komppula, M.: Optical and geometrical aerosol particle properties over the United Arab Emirates, *Atmos. Chem. Phys.*, 20, 8909–8922, <https://doi.org/10.5194/acp-20-8909-2020>, 2020.
- Flament, T., Traçon, D., Lacour, A., Dabas, A., Ehlers, F., and Huber, D.: Aeolus L2A aerosol optical properties product: standard correct  
670 algorithm and Mie correct algorithm, *Atmos. Meas. Tech.*, 14, 7851–7871, <https://doi.org/10.5194/amt-14-7851-2021>, 2021.
- Floutsi, A. A., Baars, H., and Wandinger, U.: Towards an automatic aerosol typing algorithm applicable for ground-based and spaceborne lidars, *Living Planet Symposium*, <https://doi.org/10.13140/RG.2.2.14147.45604>, 2019.



- Floutsi, A. A., Baars, H., Radenz, M., Haarig, M., Yin, Z., Seifert, P., Jimenez, C., Ansmann, A., Engelmann, R., Barja, B., Zamorano, F., and Wandinger, U.: Advection of Biomass Burning Aerosols towards the Southern Hemispheric Mid-Latitude Station of Punta Arenas as  
675 Observed with Multiwavelength Polarization Raman Lidar, *Remote Sens.*, 13, 138, <https://doi.org/10.3390/rs13010138>, 2021.
- Freudenthaler, V.: About the effects of polarising optics on lidar signals and the  $\Delta 90$  calibration, *Atmos. Meas. Tech.*, 9, 4181–4255, <https://doi.org/10.5194/amt-9-4181-2016>, 2016.
- Freudenthaler, V., Linné, H., Chaikovski, A., Rabus, D., and Groß, S.: EARLINET lidar quality assurance tools, *Atmos. Meas. Tech. Discuss.*, 2018, 1–35, <https://doi.org/10.5194/amt-2017-395>, 2018.
- 680 Giannakaki, E., van Zyl, P. G., Müller, D., Balis, D., and Komppula, M.: Optical and microphysical characterization of aerosol layers over South Africa by means of multi-wavelength depolarization and Raman lidar measurements, *Atmos. Chem. Phys.*, 16, 8109–8123, <https://doi.org/10.5194/acp-16-8109-2016>, 2016.
- Griesche, H. J., Seifert, P., Ansmann, A., Baars, H., Barrientos Velasco, C., Bühl, J., Engelmann, R., Radenz, M., Zhenping, Y., and Macke, A.: Application of the shipborne remote sensing supersite OCEANET for profiling of Arctic aerosols and clouds during Polarstern cruise  
685 PS106, *Atmos. Meas. Tech.*, 13, 5335–5358, <https://doi.org/10.5194/amt-13-5335-2020>, 2020.
- Groß, S., Freudenthaler, V., Toledano, C., Seefeldner, M., and Wiegner, M.: Mini-lidar measurements of particle depolarization and Raman scattering of Saharan-dust and biomass burning at 355 nm during SAMUM 2, *Proceedings of 24th International Laser Radar Conference (ILRC 24)*, pp. 23–27, 2008.
- Groß, S., Tesche, M., Freudenthaler, V., Toledano, C., Wiegner, M., Ansmann, A., Althausen, D., and Seefeldner, M.: Characterization of  
690 Saharan dust, marine aerosols and mixtures of biomass-burning aerosols and dust by means of multi-wavelength depolarization and Raman lidar measurements during SAMUM–2, *Tellus B*, 63, 706–724, <https://doi.org/10.1111/j.1600-0889.2011.00556.x>, 2011.
- Groß, S., Freudenthaler, V., Wiegner, M., Gasteiger, J., Geiß, A., and Schnell, F.: Dual-wavelength linear depolarization ratio of volcanic aerosols: Lidar measurements of the Eyjafjallajökull plume over Maisach, Germany, *Atmos. Environ.*, 48, 85–96, <https://doi.org/10.1016/j.atmosenv.2011.06.017>, 2012.
- 695 Groß, S., Esselborn, M., Weinzierl, B., Wirth, M., Fix, A., and Petzold, A.: Aerosol classification by airborne high spectral resolution lidar observations, *Atmos. Chem. Phys.*, 13, 2487–2505, <https://doi.org/10.5194/acp-13-2487-2013>, 2013.
- Groß, S., Freudenthaler, V., Schepanski, K., Toledano, C., Schäfler, A., Ansmann, A., and Weinzierl, B.: Optical properties of long-range transported Saharan dust over Barbados as measured by dual-wavelength depolarization Raman lidar measurements, *Atmos. Chem. Phys.*, 15, 11 067–11 080, <https://doi.org/10.5194/acp-15-11067-2015>, 2015.
- 700 Haarig, M., Engelmann, R., Ansmann, A., Veselovskii, I., Whiteman, D. N., and Althausen, D.: 1064 nm rotational Raman lidar for particle extinction and lidar-ratio profiling: cirrus case study, *Atmos. Meas. Tech.*, 9, 4269–4278, <https://doi.org/10.5194/amt-9-4269-2016>, 2016.
- Haarig, M., Ansmann, A., Althausen, D., Klepel, A., Groß, S., Freudenthaler, V., Toledano, C., Mamouri, R. E., Farrell, D. A., Prescod, D. A., Marinou, E., Burton, S. P., Gasteiger, J., Engelmann, R., and Baars, H.: Triple-wavelength depolarization-ratio profiling of Saharan dust over Barbados during SALTRACE in 2013 and 2014, *Atmos. Chem. Phys.*, 17, 10 767–10 794, <https://doi.org/10.5194/acp-17-10767-2017>, 2017a.
- 705 Haarig, M., Ansmann, A., Gasteiger, J., Kandler, K., Althausen, D., Baars, H., Radenz, M., and Farrell, D. A.: Dry versus wet marine particle optical properties: RH dependence of depolarization ratio, backscatter, and extinction from multiwavelength lidar measurements during SALTRACE, *Atmos. Chem. Phys.*, 17, 14 199–14 217, <https://doi.org/10.5194/acp-17-14199-2017>, 2017b.



- Haarig, M., Ansmann, A., Baars, H., Jimenez, C., Veselovskii, I., Engelmann, R., and Althausen, D.: Depolarization and lidar ratios at 355,  
710 532, and 1064 nm and microphysical properties of aged tropospheric and stratospheric Canadian wildfire smoke, *Atmos. Chem. Phys.*,  
18, 11 847–11 861, <https://doi.org/10.5194/acp-18-11847-2018>, 2018.
- Haarig, M., Walser, A., Ansmann, A., Dollner, M., Althausen, D., Sauer, D., Farrell, D., and Weinzierl, B.: Profiles of cloud condensation  
nuclei, dust mass concentration, and ice-nucleating-particle-relevant aerosol properties in the Saharan Air Layer over Barbados from  
715 polarization lidar and airborne in situ measurements, *Atmos. Chem. Phys.*, 19, 13 773–13 788, [https://doi.org/10.5194/acp-19-13773-](https://doi.org/10.5194/acp-19-13773-2019)  
2019, 2019.
- Haarig, M., Ansmann, A., Engelmann, R., Baars, H., Toledano, C., Torres, B., Althausen, D., Radenz, M., and Wandinger, U.: First triple-  
wavelength lidar observations of depolarization and extinction-to-backscatter ratios of Saharan dust, *Atmos. Chem. Phys.*, 22, 355–369,  
<https://doi.org/10.5194/acp-22-355-2022>, 2022.
- Hansen, J., Sato, M., and Ruedy, R.: Radiative forcing and climate response, *J. Geophys. Res.-Atmos.*, 102, 6831–6864,  
720 <https://doi.org/10.1029/96JD03436>, 1997.
- Heese, B., Althausen, D., Baars, H., Bohlmann, S., and Deng, R.: Aerosol Properties over Southeastern China from Multi-Wavelength Raman  
and Depolarization Lidar Measurements, *EPJ Web Conf.*, Proceedings of the 27th International Laser Radar Conference (ILRC 27), 119,  
<https://doi.org/10.1051/epjconf/201611923018>, 2016.
- Heese, B., Baars, H., Bohlmann, S., Althausen, D., and Deng, R.: Continuous vertical aerosol profiling with a multi-wavelength Raman  
725 polarization lidar over the Pearl River Delta, China, *Atmos. Chem. Phys.*, 17, 6679–6691, <https://doi.org/10.5194/acp-17-6679-2017>,  
2017.
- Heese, B., Floutsi, A. A., Baars, H., Althausen, D., Hofer, J., Herzog, A., Mewes, S., Radenz, M., and Schechner, Y. Y.: The vertical  
aerosol type distribution above Israel – 2 years of lidar observations at the coastal city of Haifa, *Atmos. Chem. Phys.*, 22, 1633–1648,  
<https://doi.org/10.5194/acp-22-1633-2022>, 2022.
- 730 Herold, C., Althausen, D., Müller, D., Tesche, M., Seifert, P., Engelmann, R., Flamant, C., Bhawar, R., and Girolamo, P. D.: Compari-  
son of Raman Lidar Observations of Water Vapor with COSMO-DE Forecasts during COPS 2007, *Weath. and For.*, 26, 1056 – 1066,  
<https://doi.org/10.1175/2011WAF2222448.1>, 2011.
- Hofer, J., Althausen, D., Abdullaev, S. F., Makhmudov, A. N., Nazarov, B. I., Schettler, G., Engelmann, R., Baars, H., Fomba, K. W.,  
Müller, K., Heinold, B., Kandler, K., and Ansmann, A.: Long-term profiling of mineral dust and pollution aerosol with multiwave-  
735 length polarization Raman lidar at the Central Asian site of Dushanbe, Tajikistan: case studies, *Atmos. Chem. Phys.*, 17, 14 559–14 577,  
<https://doi.org/10.5194/acp-17-14559-2017>, 2017.
- Hofer, J., Ansmann, A., Althausen, D., Engelmann, R., Baars, H., Fomba, K. W., Wandinger, U., Abdullaev, S. F., and Makhmudov, A. N.:  
Optical properties of Central Asian aerosol relevant for spaceborne lidar applications and aerosol typing at 355 and 532 nm, *Atmos. Chem.*  
*Phys.*, 20, 9265–9280, <https://doi.org/10.5194/acp-20-9265-2020>, 2020.
- 740 Hänel, A., Baars, H., Althausen, D., Ansmann, A., Engelmann, R., and Sun, J. Y.: One-year aerosol profiling with EUCAARI Raman lidar at  
Shangdianzi GAW station: Beijing plume and seasonal variations, *J. Geophys. Res.-Atmos.*, 117, <https://doi.org/10.1029/2012JD017577>,  
2012.
- Illingworth, A. J., Barker, H. W., Beljaars, A., Ceccaldi, M., Chepfer, H., Clerbaux, N., Cole, J., Delanoe, J., Domenech, C., Donovan, D. P.,  
Fukuda, S., Hiraoka, M., Hogan, R. J., Huenerbein, A., Kollias, P., Kubota, T., Nakajima, T., Nakajima, T. Y., Nishizawa, T., Ohno, Y.,  
745 Okamoto, H., Oki, R., Sato, K., Satoh, M., Shephard, M. W., Velazquez-Blazquez, A., Wandinger, U., Wehr, T., and van Zadelhoff, G. J.:



- THE EARTHCARE SATELLITE The Next Step Forward in Global Measurements of Clouds, Aerosols, Precipitation, and Radiation, B. Am. Meteorol. Soc., 96, 1311–1332, <https://doi.org/10.1175/bams-d-12-00227.1>, 2015.
- 750 Janicka, L., Stachlewska, I. S., Markowicz, K. M., Baars, H., Engelmann, R., and Heese, B.: Lidar Measurements of Canadian Forest Fire Smoke Episode Observed in July 2013 over Warsaw, Poland, EPJ Web Conf., Proceedings of the 27th International Laser Radar Conference (ILRC 27), 119, <https://doi.org/10.1051/epjconf/201611918005>, 2016.
- Janicka, L., Stachlewska, I. S., Veselovskii, I., and Baars, H.: Temporal variations in optical and microphysical properties of mineral dust and biomass burning aerosol derived from daytime Raman lidar observations over Warsaw, Poland, Atmos. Environ., 169, 162–174, <https://doi.org/10.1016/j.atmosenv.2017.09.022>, 2017.
- 755 Jimenez, C., Ansmann, A., Engelmann, R., Haarig, M., Schmidt, J., and Wandinger, U.: Polarization lidar: an extended three-signal calibration approach, Atmos. Meas. Tech., 12, 1077–1093, <https://doi.org/10.5194/amt-12-1077-2019>, 2019.
- Jimenez, C., Ansmann, A., Engelmann, R., Donovan, D., Malinka, A., Schmidt, J., Seifert, P., and Wandinger, U.: The dual-field-of-view polarization lidar technique: a new concept in monitoring aerosol effects in liquid-water clouds – theoretical framework, Atmos. Chem. Phys., 20, 15 247–15 263, <https://doi.org/10.5194/acp-20-15247-2020>, 2020a.
- 760 Jimenez, C., Ansmann, A., Engelmann, R., Donovan, D., Malinka, A., Seifert, P., Wiesen, R., Radenz, M., Yin, Z., Bühl, J., Schmidt, J., Barja, B., and Wandinger, U.: The dual-field-of-view polarization lidar technique: a new concept in monitoring aerosol effects in liquid-water clouds – case studies, Atmos. Chem. Phys., 20, 15 265–15 284, <https://doi.org/10.5194/acp-20-15265-2020>, 2020b.
- Kaduk, C.: Characterization of the optical properties of complex aerosol mixtures observed with a multiwavelength–Raman–polarization lidar during the 6–weeks BACCCHUS campaign in Cyprus in spring 2015, MSc thesis, Leipzig University, [https://www.tropos.de/fileadmin/user\\_upload/Institut/Abteilungen/Fernerkundung/Daten\\_PDF/MA\\_Clara\\_Kaduk.pdf](https://www.tropos.de/fileadmin/user_upload/Institut/Abteilungen/Fernerkundung/Daten_PDF/MA_Clara_Kaduk.pdf), (last access: 18 October 2022), 2017.
- 765 Kanitz, T.: Vertical distribution of aerosols above the Atlantic Ocean, Punta Arenas (Chile), and Stellenbosch (South Africa), PhD dissertation, Technische Universität Berlin, <https://doi.org/10.14279/depositonce-3386>, 2012.
- Kanitz, T., Ansmann, A., Engelmann, R., and Althausen, D.: North-south cross sections of the vertical aerosol distribution over the Atlantic Ocean from multiwavelength Raman/polarization lidar during Polarstern cruises, J. Geophys. Res.-Atmos., 118, 2643–2655, <https://doi.org/10.1002/jgrd.50273>, 2013a.
- 770 Kanitz, T., Ansmann, A., Seifert, P., Engelmann, R., Kalisch, J., and Althausen, D.: Radiative effect of aerosols above the northern and southern Atlantic Ocean as determined from shipborne lidar observations, J. Geophys. Res.-Atmos., 118, 12 556–12 565, <https://doi.org/10.1002/2013jd019750>, 2013b.
- 775 Kanitz, T., Ansmann, A., Foth, A., Seifert, P., Wandinger, U., Engelmann, R., Baars, H., Althausen, D., Casiccia, C., and Zamorano, F.: Surface matters: limitations of CALIPSO V3 aerosol typing in coastal regions, Atmos. Meas. Tech., 7, 2061–2072, <https://doi.org/10.5194/amt-7-2061-2014>, 2014a.
- Kanitz, T., Engelmann, R., Heinold, B., Baars, H., Skupin, A., and Ansmann, A.: Tracking the Saharan Air Layer with shipborne lidar across the tropical Atlantic, Geophys. Res. Lett., 41, 1044–1050, <https://doi.org/10.1002/2013GL058780>, 2014b.
- 780 Kim, M. H., Omar, A. H., Tackett, J. L., Vaughan, M. A., Winker, D. M., Trepte, C. R., Hu, Y. X., Liu, Z. Y., Poole, L. R., Pitts, M. C., Kar, J., and Magill, B. E.: The CALIPSO version 4 automated aerosol classification and lidar ratio selection algorithm, Atmos. Meas. Tech., 11, 6107–6135, <https://doi.org/10.5194/amt-11-6107-2018>, 2018.
- Komppula, M., Mielonen, T., Arola, A., Korhonen, K., Lihavainen, H., Hyvärinen, A. P., Baars, H., Engelmann, R., Althausen, D., Ansmann, A., Müller, D., Panwar, T. S., Hooda, R. K., Sharma, V. P., Kerminen, V. M., Lehtinen, K. E. J., and Viisanen, Y.: Technical Note: One



- year of Raman-lidar measurements in Gual Pahari EUCAARI site close to New Delhi in India – Seasonal characteristics of the aerosol vertical structure, *Atmos. Chem. Phys.*, 12, 4513–4524, <https://doi.org/10.5194/acp-12-4513-2012>, 2012.
- 785 Kulmala, M., Asmi, A., Lappalainen, H. K., Baltensperger, U., Brenguier, J. L., Facchini, M. C., Hansson, H. C., Hov, o., O’Dowd, C. D., Pöschl, U., Wiedensohler, A., Boers, R., Boucher, O., de Leeuw, G., Denier van der Gon, H. A. C., Feichter, J., Krejci, R., Laj, P., Lihavainen, H., Lohmann, U., McFiggans, G., Mentel, T., Pilinis, C., Riipinen, I., Schulz, M., Stohl, A., Swietlicki, E., Vignati, E., Alves, C., Amann, M., Ammann, M., Arabas, S., Artaxo, P., Baars, H., Beddows, D. C. S., Bergström, R., Beukes, J. P., Bilde, M., Burkhart, J. F., Canonaco, F., Clegg, S. L., Coe, H., Crumeyrolle, S., D’Anna, B., Decesari, S., Gilardoni, S., Fischer, M., Fjaeraa, A. M.,
- 790 Fountoukis, C., George, C., Gomes, L., Halloran, P., Hamburger, T., Harrison, R. M., Herrmann, H., Hoffmann, T., Hoose, C., Hu, M., Hyvärinen, A., Hörrak, U., Iinuma, Y., Iversen, T., Josipovic, M., Kanakidou, M., Kiendler-Scharr, A., Kirkevåg, A., Kiss, G., Klimont, Z., Kolmonen, P., Komppula, M., Kristjánsson, J. E., Laakso, L., Laaksonen, A., Labonnote, L., Lanz, V. A., Lehtinen, K. E. J., Rizzo, L. V., Makkonen, R., Manninen, H. E., McMeeking, G., Merikanto, J., Minikin, A., Mirme, S., Morgan, W. T., Nemitz, E., O’Donnell, D., Panwar, T. S., Pawlowska, H., Petzold, A., Pienaar, J. J., Pio, C., Plass-Duelmer, C., Prévôt, A. S. H., Pryor, S., Reddington, C. L.,
- 795 Roberts, G., Rosenfeld, D., Schwarz, J., Seland, o., Sellegri, K., et al.: General overview: European Integrated project on Aerosol Cloud Climate and Air Quality interactions (EUCAARI) – integrating aerosol research from nano to global scales, *Atmos. Chem. Phys.*, 11, 13 061–13 143, <https://doi.org/10.5194/acp-11-13061-2011>, 2011.
- Lelieveld, J., Hadjinicolaou, P., Kostopoulou, E., Chenoweth, J., El Maayar, M., Giannakopoulos, C., Hannides, C., Lange, M. A., Tanarhte, M., Tyrlis, E., and Xoplaki, E.: Climate change and impacts in the Eastern Mediterranean and the Middle East, *Clim. Change*, 114, 667–687, <https://doi.org/10.1007/s10584-012-0418-4>, 2012.
- 800 Mamouri, R. E. and Ansmann, A.: Fine and coarse dust separation with polarization lidar, *Atmos. Meas. Tech.*, 7, 3717–3735, <https://doi.org/10.5194/amt-7-3717-2014>, 2014.
- Mamouri, R. E. and Ansmann, A.: Estimated desert-dust ice nuclei profiles from polarization lidar: methodology and case studies, *Atmos. Chem. Phys.*, 15, 3463–3477, <https://doi.org/10.5194/acp-15-3463-2015>, 2015.
- 805 Mamouri, R. E. and Ansmann, A.: Potential of polarization lidar to provide profiles of CCN- and INP-relevant aerosol parameters, *Atmos. Chem. Phys.*, 16, 5905–5931, <https://doi.org/10.5194/acp-16-5905-2016>, 2016.
- Mattis, I., Ansmann, A., Althausen, D., Jaenisch, V., Wandinger, U., Müller, D., Arshinov, Y. F., Bobrovnikov, S. M., and Serikov, I. B.: Relative-humidity profiling in the troposphere with a Raman lidar, *Appl. Opt.*, 41, 6451–6462, <https://doi.org/10.1364/AO.41.006451>, 2002a.
- 810 Mattis, I., Ansmann, A., Müller, D., Wandinger, U., and Althausen, D.: Dual-wavelength Raman lidar observations of the extinction-to-backscatter ratio of Saharan dust, *Geophys. Res. Lett.*, 29, <https://doi.org/10.1029/2002GL014721>, 2002b.
- Mattis, I., Ansmann, A., Müller, D., Wandinger, U., and Althausen, D.: Multiyear aerosol observations with dual-wavelength Raman lidar in the framework of EARLINET, *J. Geophys. Res.-Atmos.*, 109, <https://doi.org/10.1029/2004JD004600>, 2004.
- Mattis, I., Müller, D., Ansmann, A., Wandinger, U., Preißler, J., Seifert, P., and Tesche, M.: Ten years of multiwavelength Raman lidar
- 815 observations of free-tropospheric aerosol layers over central Europe: Geometrical properties and annual cycle, *J. Geophys. Res.-Atmos.*, 113, <https://doi.org/https://doi.org/10.1029/2007JD009636>, 2008.
- Müller, D., Wandinger, U., Althausen, D., Mattis, I., and Ansmann, A.: Retrieval of physical particle properties from lidar observations of extinction and backscatter at multiple wavelengths, *Appl. Opt.*, 37, 2260–2263, <https://doi.org/10.1364/AO.37.002260>, 1998.
- Müller, D., Wandinger, U., and Ansmann, A.: Microphysical particle parameters from extinction and backscatter lidar data by inversion with
- 820 regularization: theory, *Appl. Opt.*, 38, 2346–2357, <https://doi.org/10.1364/AO.38.002346>, 1999a.



- Müller, D., Wandinger, U., and Ansmann, A.: Microphysical particle parameters from extinction and backscatter lidar data by inversion with regularization: simulation, *Appl. Opt.*, 38, 2358–2368, <https://doi.org/10.1364/AO.38.002358>, 1999b.
- Müller, D., Wagner, F., Wandinger, U., Ansmann, A., Wendisch, M., Althausen, D., and von Hoyningen-Huene, W.: Microphysical particle parameters from extinction and backscatter lidar data by inversion with regularization: experiment, *Appl. Opt.*, 39, 1879–1892, <https://doi.org/10.1364/AO.39.001879>, 2000.
- 825 Müller, D., Kolgotin, A., Mattis, I., Petzold, A., and Stohl, A.: Vertical profiles of microphysical particle properties derived from inversion with two-dimensional regularization of multiwavelength Raman lidar data: experiment, *Appl. Opt.*, 50, 2069–2079, <https://doi.org/10.1364/AO.50.002069>, 2011.
- Müller, D., Ansmann, A., Wagner, F., Franke, K., and Althausen, D.: European pollution outbreaks during ACE 2: Microphysical particle properties and single-scattering albedo inferred from multiwavelength lidar observations, *J. Geophys. Res.-Atmos.*, 107, <https://doi.org/10.1029/2001JD001110>, 2002.
- 830 Müller, D., Franke, K., Ansmann, A., Althausen, D., and Wagner, F.: Indo-Asian pollution during INDOEX: Microphysical particle properties and single-scattering albedo inferred from multiwavelength lidar observations, *J. Geophys. Res.-Atmos.*, 108, <https://doi.org/10.1029/2003JD003538>, 2003.
- 835 Müller, D., Mattis, I., Wandinger, U., Ansmann, A., Althausen, D., and Stohl, A.: Raman lidar observations of aged Siberian and Canadian forest fire smoke in the free troposphere over Germany in 2003: Microphysical particle characterization, *J. Geophys. Res.-Atmos.*, 110, 16, <https://doi.org/10.1029/2004jd005756>, 2005.
- Müller, D., Ansmann, A., Mattis, I., Tesche, M., Wandinger, U., Althausen, D., and Pisani, G.: Aerosol-type-dependent lidar ratios observed with Raman lidar, *J. Geophys. Res.-Atmos.*, 112, <https://doi.org/10.1029/2006jd008292>, 2007.
- 840 Nicolae, D., Vasilescu, J., Talianu, C., Biniotoglou, I., Nicolae, V., Andrei, S., and Antonescu, B.: A neural network aerosol-typing algorithm based on lidar data, *Atmos. Chem. Phys.*, 18, 14 511–14 537, <https://doi.org/10.5194/acp-18-14511-2018>, 2018.
- Ohneiser, K., Ansmann, A., Baars, H., Seifert, P., Barja, B., Jimenez, C., Radenz, M., Teisseire, A., Floutsi, A., Haarig, M., Foth, A., Chudnovsky, A., Engelmann, R., Zamorano, F., Bühl, J., and Wandinger, U.: Smoke of extreme Australian bushfires observed in the stratosphere over Punta Arenas, Chile, in January 2020: optical thickness, lidar ratios, and depolarization ratios at 355 and 532 nm, *Atmos. Chem. Phys.*, 20, 8003–8015, <https://doi.org/10.5194/acp-20-8003-2020>, 2020.
- 845 Ohneiser, K., Ansmann, A., Chudnovsky, A., Engelmann, R., Ritter, C., Veselovskii, I., Baars, H., Gebauer, H., Griesche, H., Radenz, M., Hofer, J., Althausen, D., Dahlke, S., and Maturilli, M.: The unexpected smoke layer in the High Arctic winter stratosphere during MOSAiC 2019–2020, *Atmos. Chem. Phys.*, 21, 15 783–15 808, <https://doi.org/10.5194/acp-21-15783-2021>, 2021.
- Omar, A. H., Won, J.-G., Winker, D. M., Yoon, S.-C., Dubovik, O., and McCormick, M. P.: Development of global aerosol models using cluster analysis of Aerosol Robotic Network (AERONET) measurements, *J. Geophys. Res.-Atmos.*, 110, <https://doi.org/10.1029/2004JD004874>, 2005.
- 850 Omar, A. H., Winker, D. M., Vaughan, M. A., Hu, Y., Trepte, C. R., Ferrare, R. A., Lee, K.-P., Hostetler, C. A., Kittaka, C., Rogers, R. R., Kuehn, R. E., and Liu, Z.: The CALIPSO Automated Aerosol Classification and Lidar Ratio Selection Algorithm, *J. Atmos. Ocean. Tech.*, 26, 1994–2014, <https://doi.org/10.1175/2009jtecha1231.1>, 2009.
- 855 Papagiannopoulos, N., Mona, L., Amodeo, A., D’Amico, G., Gumà Claramunt, P., Pappalardo, G., Alados-Arboledas, L., Guerrero-Rascado, J. L., Amiridis, V., Kokkalis, P., Apituley, A., Baars, H., Schwarz, A., Wandinger, U., Biniotoglou, I., Nicolae, D., Bortoli, D., Comerón, A., Rodríguez-Gómez, A., Sicard, M., Papayannis, A., and Wiegner, M.: An automatic observation-based aerosol typing method for EARLINET, *Atmos. Chem. Phys.*, 18, 15 879–15 901, <https://doi.org/10.5194/acp-18-15879-2018>, 2018.



- Pappalardo, G., Amodeo, A., Apituley, A., Comeron, A., Freudenthaler, V., Linné, H., Ansmann, A., Bösenberg, J., D'Amico, G., Mattis, I.,  
860 Mona, L., Wandinger, U., Amiridis, V., Alados-Arboledas, L., Nicolae, D., and Wiegner, M.: EARLINET: towards an advanced sustainable  
European aerosol lidar network, *Atmos. Meas. Tech.*, 7, 2389–2409, <https://doi.org/10.5194/amt-7-2389-2014>, 2014.
- Pereira, N. S., Preißler, J., Guerrero-Rascado, J. L., Silva, A. M., and Wagner, F.: Forest Fire Smoke Layers Observed in the Free Tro-  
posphere over Portugal with a Multiwavelength Raman Lidar: Optical and Microphysical Properties, *Sc. World J.*, 2014, 421 838,  
<https://doi.org/10.1155/2014/421838>, 2014.
- 865 Preißler, J., Wagner, F., Pereira, S. N., and Guerrero-Rascado, J. L.: Multi-instrumental observation of an exceptionally strong Saharan dust  
outbreak over Portugal, *J. Geophys. Res.-Atmos.*, 116, <https://doi.org/10.1029/2011JD016527>, 2011.
- Preißler, J., Wagner, F., Guerrero-Rascado, J. L., and Silva, A. M.: Two years of free-tropospheric aerosol layers observed over Portugal by  
lidar, *J. Geophys. Res.-Atmos.*, 118, 3676–3686, <https://doi.org/10.1002/jgrd.50350>, 2013.
- Radenz, M., Bühl, J., Seifert, P., Baars, H., Engelmann, R., Barja González, B., Mamouri, R. E., Zamorano, F., and Ansmann, A.: Hemispheric  
870 contrasts in ice formation in stratiform mixed-phase clouds: disentangling the role of aerosol and dynamics with ground-based remote  
sensing, *Atmos. Chem. Phys.*, 21, 17 969–17 994, <https://doi.org/10.5194/acp-21-17969-2021>, 2021a.
- Radenz, M., Seifert, P., Baars, H., Floutsis, A. A., Yin, Z., and Bühl, J.: Automated time–height-resolved air mass source attribution for  
profiling remote sensing applications, *Atmos. Chem. Phys.*, 21, 3015–3033, <https://doi.org/10.5194/acp-21-3015-2021>, 2021b.
- Ramanathan, V., Crutzen, P. J., Lelieveld, J., Mitra, A. P., Althausen, D., Anderson, J., Andreae, M. O., Cantrell, W., Cass, G. R., Chung,  
875 C. E., Clarke, A. D., Coakley, J. A., Collins, W. D., Conant, W. C., Dulac, F., Heintzenberg, J., Heymsfield, A. J., Holben, B., Howell, S.,  
Hudson, J., Jayaraman, A., Kiehl, J. T., Krishnamurti, T. N., Lubin, D., McFarquhar, G., Novakov, T., Ogren, J. A., Podgorny, I. A., Prather,  
K., Priestley, K., Prospero, J. M., Quinn, P. K., Rajeev, K., Rasch, P., Rupert, S., Sadourny, R., Satheesh, S. K., Shaw, G. E., Sheridan, P.,  
and Valero, F. P. J.: Indian Ocean Experiment: An integrated analysis of the climate forcing and effects of the great Indo-Asian haze, *J.*  
*Geophys. Res.-Atmos.*, 106, 28 371–28 398, <https://doi.org/10.1029/2001JD900133>, 2001.
- 880 Rittmeister, F., Ansmann, A., Engelmann, R., Skupin, A., Baars, H., Kanitz, T., and Kinne, S.: Profiling of Saharan dust from the Caribbean to  
western Africa – Part 1: Layering structures and optical properties from shipborne polarization/Raman lidar observations, *Atmos. Chem.*  
*Phys.*, 17, 12 963–12 983, <https://doi.org/10.5194/acp-17-12963-2017>, 2017.
- Sasano, Y. and Browell, E. V.: Light scattering characteristics of various aerosol types derived from multiple wavelength lidar observations,  
*Appl. Opt.*, 28, 1670–1679, <https://doi.org/10.1364/AO.28.001670>, 1989.
- 885 Schmidt, J., Wandinger, U., and Malinka, A.: Dual-field-of-view Raman lidar measurements for the retrieval of cloud microphysical proper-  
ties, *Appl. Opt.*, 52, 2235–2247, <https://doi.org/10.1364/AO.52.002235>, 2013.
- Schuster, G., Toth, T., Trepte, C., Chin, M., Bian, H., Kim, D., Kar, J., and Welton, E.: Mapping Modeled Aerosol Species to Measured Lidar  
Ratios for the MIRA Project, The 30th International Laser Radar Conference, 2022.
- Sicard, M., Guerrero-Rascado, J. L., Navas-Guzmán, F., Preißler, J., Molero, F., Tomás, S., Bravo-Aranda, J. A., Comerón, A., Rocadenbosch,  
890 F., Wagner, F., Pujadas, M., and Alados-Arboledas, L.: Monitoring of the Eyjafjallajökull volcanic aerosol plume over the Iberian Peninsula  
by means of four EARLINET lidar stations, *Atmos. Chem. Phys.*, 12, 3115–3130, <https://doi.org/10.5194/acp-12-3115-2012>, 2012.
- Stoffelen, A., Pailleux, J., Källén, E., Vaughan, J. M., Isaksen, I., Flamant, P., Wergen, W., Andersson, E., Schyberg, H., Culoma, A., Meynart,  
R., Endemann, M., and Ingmann, P.: The Atmospheric Dynamics Mission For Global Wind Field Measurement, *B. Am. Meteorol. Soc.*,  
86, 73 – 88, <https://doi.org/10.1175/BAMS-86-1-73>, 2005.



- 895 Sugimoto, N., Matsui, I., Shimizu, A., Uno, I., Asai, K., Endoh, T., and Nakajima, T.: Observation of dust and anthropogenic aerosol plumes in the Northwest Pacific with a two-wavelength polarization lidar on board the research vessel Mirai, *Geophys. Res. Lett.*, 29, 7–1–7–4, <https://doi.org/10.1029/2002GL015112>, 2002.
- Sugimoto, N., Nishizawa, T., Shimizu, A., Matsui, I., and Jin, Y.: Characterization of aerosols in East Asia with the Asian Dust and Aerosol Lidar Observation Network (AD-Net), vol. 9262 of *SPIE Asia-Pacific Remote Sensing*, SPIE, <https://doi.org/10.1117/12.2069892>, 2014.
- 900 Szczepanik, D. M., Stachlewska, I. S., Tetoni, E., and Althausen, D.: Properties of Saharan Dust Versus Local Urban Dust—A Case Study, *Earth and Space Sc.*, 8, e2021EA001 816, <https://doi.org/10.1029/2021EA001816>, 2021.
- Tesche, M.: Vertical profiling of aerosol optical properties with multiwavelength aerosol lidar during the Saharan Mineral Dust Experiments, PhD dissertation, University of Leipzig, <https://nbn-resolving.org/urn:nbn:de:bsz:15-qucosa-71257>, (last access: 18 October 2022), 2011.
- Tesche, M., Ansmann, A., Müller, D., Althausen, D., Engelmann, R., Hu, M., and Zhang, Y.: Particle backscatter, extinction, and lidar ratio  
905 profiling with Raman lidar in south and north China, *Appl. Opt.*, 46, 6302–6308, <https://doi.org/10.1364/AO.46.006302>, 2007.
- Tesche, M., Ansmann, A., Müller, D., Althausen, D., Mattis, I., Heese, B., Freudenthaler, V., Wiegner, M., Esselborn, M., Pisani, G., and Knippertz, P.: Vertical profiling of Saharan dust with Raman lidars and airborne HSRL in southern Morocco during SAMUM, *Tellus B*, 61, 144–164, <https://doi.org/10.1111/j.1600-0889.2008.00390.x>, 2009a.
- Tesche, M., Ansmann, A., Müller, D., Althausen, D., Engelmann, R., Freudenthaler, V., and Groß, S.: Vertically resolved separation of dust  
910 and smoke over Cape Verde using multiwavelength Raman and polarization lidars during Saharan Mineral Dust Experiment 2008, *J. Geophys. Res.-Atmos.*, 114, 14, <https://doi.org/10.1029/2009jd011862>, 2009b.
- Tesche, M., Groß, S., Ansmann, A., Müller, D., Althausen, D., Freudenthaler, V., and Esselborn, M.: Profiling of Saharan dust and biomass-burning smoke with multiwavelength polarization Raman lidar at Cape Verde, *Tellus B*, 63, 649–676, <https://doi.org/10.1111/j.1600-0889.2011.00548.x>, 2011a.
- 915 Tesche, M., Müller, D., Groß, S., Ansmann, A., Althausen, D., Freudenthaler, V., Weinzierl, B., Veira, A., and Petzold, A.: Optical and microphysical properties of smoke over Cape Verde inferred from multiwavelength lidar measurements, *Tellus B*, 63, 677–694, <https://doi.org/10.1111/j.1600-0889.2011.00549.x>, 2011b.
- Urbanneck, C.: Retrieval of aerosol optical and microphysical properties in Cyprus during A-LIFE and CyCARE by lidar and closure studies with airborne in-situ measurements – Towards aerosol-cloud interaction investigations, MSc thesis, Leipzig University, [https://www.tropos.de/fileadmin/user\\_upload/Institut/Abteilungen/Fernerkundung/Daten\\_PDF/MA\\_claudia\\_urbanneck.pdf](https://www.tropos.de/fileadmin/user_upload/Institut/Abteilungen/Fernerkundung/Daten_PDF/MA_claudia_urbanneck.pdf), (last access: 18 October 2022), 2018.
- 920 Wandinger, U., Baars, H., Engelmann, R., Hünerbein, A., Horn, S., Kanitz, T., Donovan, D., van Zadelhoff, G.-J., Daou, D., Fischer, J., von Bismarck, J., Filipitsch, F., Docter, N., Eisinger, M., Lajas, D., and Wehr, T.: HETEAC: The Aerosol Classification Model for EarthCARE, *EPJ Web Conf.*, Proceedings of the 27th International Laser Radar Conference (ILRC 27), 119, 01 004, <https://doi.org/10.1051/epjconf/201611901004>, 2016a.
- 925 Wandinger, U., Freudenthaler, V., Baars, H., Amodeo, A., Engelmann, R., Mattis, I., Groß, S., Pappalardo, G., Giunta, A., D’Amico, G., Chaikovskiy, A., Osipenko, F., Slesar, A., Nicolae, D., Belegante, L., Talianu, C., Serikov, I., Linne, H., Jansen, F., Apituley, A., Wilson, K. M., de Graaf, M., Trickl, T., Giehl, H., Adam, M., Comeron, A., Munoz-Porcar, C., Rocadenbosch, F., Sicard, M., Tomas, S., Lange, D., Kumar, D., Pujadas, M., Molero, F., Fernandez, A. J., Alados-Arboledas, L., Bravo-Aranda, J. A., Navas-Guzman, F., Guerrero-Rascado, J. L., Granados-Munoz, M. J., Preissler, J., Wagner, F., Gausa, M., Grigorov, I., Stoyanov, D., Iarlori, M., Rizi, V., Spinelli, N., Boselli, A., Wang, X., Lo Feudo, T., Perrone, M. R., De Tomasi, F., and Burlizzi, P.: EARLINET instrument intercomparison campaigns: overview on  
930 strategy and results, *Atmos. Meas. Tech.*, 9, 1001–1023, <https://doi.org/10.5194/amt-9-1001-2016>, 2016b.



- Weinzierl, B., Sauer, D., Esselborn, M., Petzold, A., Veira, A., Rose, M., Mund, S., Wirth, M., Ansmann, A., Tesche, M., Groß, S., and Freudenthaler, V.: Microphysical and optical properties of dust and tropical biomass burning aerosol layers in the Cape Verde region—an overview of the airborne in situ and lidar measurements during SAMUM-2, *Tellus B*, 63, 589–618, <https://doi.org/10.1111/j.1600-0889.2011.00566.x>, 2011.
- Weinzierl, B., Ansmann, A., Prospero, J. M., Althausen, D., Benker, N., Chouza, F., Dollner, M., Farrell, D., Fomba, W. K., Freudenthaler, V., Gasteiger, J., Groß, S., Haarig, M., Heinold, B., Kandler, K., Kristensen, T. B., Mayol-Bracero, O. L., Müller, T., Reitebuch, O., Sauer, D., Schäfler, A., Schepanski, K., Spanu, A., Tegen, I., Toledano, C., and Walser, A.: The Saharan Aerosol Long-Range Transport and Aerosol–Cloud-Interaction Experiment: Overview and Selected Highlights, *B. Am. Meteorol. Soc.*, 98, 1427–1451, <https://doi.org/10.1175/bams-d-15-00142.1>, 2017.
- Welton, E. J., Campbell, J. R., Berkoff, T. A., Spinhirne, J. D., Tsay, S.-C., Holben, B., Shiobara, M., and Starr, D. O.: The micro-pulse lidar network (MPLNET), <https://ams.confex.com/ams/pdfpapers/86086.pdf>, (last access: 18 October 2022), 2002.
- Wendisch, M., Keil, A., Müller, D., Wandinger, U., Wendling, P., Stifter, A., Petzold, A., Fiebig, M., Wiegner, M., Freudenthaler, V., Armbruster, W., von Hoyningen-Huene, W., and Leiterer, U.: Aerosol-radiation interaction in the cloudless atmosphere during LACE 98 I. Measured and calculated broadband solar and spectral surface insulations, *J. Geophys. Res.-Atmos.*, 107, LAC 6–1–LAC 6–20, <https://doi.org/https://doi.org/10.1029/2000JD000226>, 2002.
- Winker, D. M., Vaughan, M. A., Omar, A., Hu, Y., Powell, K. A., Liu, Z., Hunt, W. H., and Young, S. A.: Overview of the CALIPSO mission and CALIOP data processing algorithms, *J. Atmos. Ocean. Tech.*, 26, 2310–2323, <https://doi.org/10.1175/2009JTECHA1281.1>, 2009.
- Yin, Z. and Baars, H.: PollyNET/Pollynet\_Processing\_Chain: Version 3.0, <https://doi.org/10.5281/zenodo.5571289>, 2021.
- Yin, Z., Ansmann, A., Baars, H., Seifert, P., Engelmann, R., Radenz, M., Jimenez, C., Herzog, A., Ohneiser, K., Hanbuch, K., Blarel, L., Goloub, P., Dubois, G., Victori, S., and Maupin, F.: Aerosol measurements with a shipborne Sun–sky–lunar photometer and collocated multiwavelength Raman polarization lidar over the Atlantic Ocean, *Atmos. Meas. Tech.*, 12, 5685–5698, <https://doi.org/10.5194/amt-12-5685-2019>, 2019.
- Zieger, P., Väisänen, O., Corbin, J. C., Partridge, D. G., Bastelberger, S., Mousavi-Fard, M., Rosati, B., Gysel, M., Krieger, U. K., Leck, C., Nenes, A., Riipinen, I., Virtanen, A., and Salter, M. E.: Revising the hygroscopicity of inorganic sea salt particles, *Nat. Comm.*, 8, 15 883, <https://doi.org/10.1038/ncomms15883>, 2017.